Netrin-1 directs vascular patterning and maturity in the developing kidney

Samuel Emery Honeycutt[1], Pierre-Emmanuel Yoann N'Guetta[1], Deanna Marie Hardesty[1], Yubin Xiong[1], Shamus Luke Cooper[1], Lori Lynn O'Brien[1*]

[1]Department of Cell Biology and Physiology

University of North Carolina at Chapel Hill, Chapel Hill, NC 27599, USA

*Corresponding author: lori_obrien@med.unc.edu

Abstract

Blood filtering by the kidney requires the establishment of an intricate vascular system that works to support body fluid and organ homeostasis. Despite these critical roles, little is known about how vascular architecture is established during kidney development. More specifically, how signals from the kidney influence vessel maturity and patterning remains poorly understood. Netrin-1 (*Ntn1*) is a secreted ligand critical for vessel and neuronal guidance. Here, we demonstrate that *Ntn1* is expressed by stromal progenitors in the developing kidney, and conditional deletion of *Ntn1* from Foxd1+ stromal progenitors ($Foxd1^{GC/+};Ntn1^{fl/fl}$) results in hypoplastic kidneys that display extended nephrogenesis. Despite expression of the netrin-1 receptor *Unc5c* in the adjacent nephron progenitor niche, *Unc5c* knockout kidneys develop normally. The netrin-1 receptor *Unc5b* is expressed by embryonic kidney endothelium and therefore we interrogated the vascular networks of $Foxd1^{GC/+};Ntn1^{fl/fl}$ kidneys. Wholemount, 3D analyses revealed the loss of a predictable vascular pattern in mutant kidneys. As vascular patterning has been linked to vessel maturity, we investigated arterialization in these mutants. Quantification of the CD31+ endothelium at E15.5 revealed no differences in metrics such as the number of branches or branch points, whereas the arterial vascular smooth muscle metrics were significantly reduced at both E15.5 and P0. In support of these results, whole kidney RNA-seq showed upregulation of angiogenic programs and downregulation of muscle-related programs which included smooth muscle-associated genes. Together, our findings highlight the significance of netrin-1 to proper vascularization and kidney development.

Keywords

Vasculature, stroma, patterning, netrin-1, kidney development

44 **Introduction**

45 The organization of blood vessels into a network capable of maintaining organ and body fluid
46 homeostasis requires both proper development of the vasculature and specialization unique to the
47 tissue. Inappropriate vascular formation and patterning can result in pathologies in many organs(Blei
48 and Bittman, 2016; Heimann and Damato, 2010; Queisser et al., 2021; Wälchli et al., 2023). Vascular
49 endothelial cells organize into branched, hierarchical networks that form a continuous system for blood
50 flow. Larger arteries branch into smaller arterioles, which further divide into capillaries. Venules then
51 return the blood to larger veins and continue its circulation(Potente and Mäkinen, 2017). The vessels
52 within these networks are distinct in their morphology and function, which is often tailored to the
53 precise needs of the organ. For example, the endothelium of the kidney glomerular capillaries and
54 ascending vasa recta are fenestrated to enable their unique functions in filtration and diffusion,
55 respectively(Molema and Aird, 2012; Pallone et al., 2003). In association with their functions, the
56 endothelium of these different vascular beds also have distinct molecular signatures(Barry et al., 2019;
57 Daniel et al., 2018). Additionally, endothelial association with mural cells delineates the various types of
58 vessels within an organ. Larger vessels such as arteries are coated by vascular smooth muscle cells
59 whereas smaller capillaries are covered by pericytes, with each type of mural cell supporting distinct
60 vascular functions(Potente and Mäkinen, 2017). Altogether, these vascular properties highlight the need
61 for precise developmental programs that support the proper formation of these complex networks.

62 Recent studies have begun to shed light on the progressive formation of kidney vascular
63 networks during development. The temporal progression and predictable rudimentary patterning of the
64 major renal arteries through mid-gestation were elucidated through comprehensive imaging
65 studies(Daniel et al., 2018; Munro et al., 2017). Arteries which connect to the aorta undergo angiogenic
66 growth towards the developing kidney forming a vascular ring around the base of the ureteric bud by

67 E11.25(Munro et al., 2017). Continued growth, remodeling, and maturation of the endothelial network
68 leads to the establishment of an arterial tree by E13.5 that forms a predictable pattern(Daniel et al.,
69 2018). Renin expressing cells are localized along the developing arterial vasculature and mark points of
70 branching, and renin itself is important for proper vascular development (Gomez et al., 1989; Reddi et
71 al., 1998; Sequeira-Lopez et al., 2015b; Takahashi et al., 2005). At the molecular level, vascular
72 patterning was shown to be regulated by the association of mural cells with the nascent endothelium
73 and modulated in part by Pbx1(Hurtado et al., 2015). Deletion of the transcription factor *Pbx1* from the
74 Foxd1+ stromal progenitors induces precocious differentiation and premature association of vascular
75 mural cells with the endothelium, leading to stochastic arterial patterning and impaired renal
76 function(Hurtado et al., 2015). Another study showed that Dicer activity in the kidney stroma is
77 important for patterning smaller vessels, such as the peritubular and glomerular capillaries(Nakagawa et
78 al., 2015). While these studies have garnered some of the first insights into how the kidney vascular
79 network is established and organized, we still lack a clear understanding of how this process is
80 modulated at the molecular level.

81 Signaling molecules play important roles during development, often providing instructional cues
82 which help pattern the developing tissues. In respect to vasculature, a number of signaling pathways,
83 which also regulate axon guidance, provide angiogenic guidance. This includes Slit/Robo, Eph/Ephrin,
84 Semaphorins/Plexin-Neuropilins, and Netrins/UNC5(Adams and Eichmann, 2010). These guidance cues
85 direct vascular development during embryogenesis, and unsurprisingly, the removal of many of these
86 cues or their receptors results in vascular defects and mortality in the forming embryo (Bin et al., 2015;
87 Gerety et al., 1999; Gitler et al., 2004; Gu et al., 2005, 2003; Jones et al., 2008; Lu et al., 2004). Netrin-1
88 (*Ntn1*) is a classical neuronal guidance cue well-known for its role in commissural axon
89 guidance(Kennedy et al., 1994; Serafini et al., 1994). However, roles for netrin-1 have expanded to
90 include mediating pancreas development, inner ear morphogenesis, mammary gland development, lung

91 branching, and angiogenesis (Larrivée et al., 2007; Liu et al., 2004; Lu et al., 2004; Salminen et al., 2000;
92 Srinivasan et al., 2003; Sun et al., 2011; Wilson et al., 2006; Yebra et al., 2003). Endothelial guidance by
93 netrin-1 is accomplished through chemotactic interactions with its cognate receptors in the vasculature,
94 Unc5b and CD146 (*Mcam1*), which regulate blood vessel growth, branching, and patterning by
95 promoting either a repulsive or attractive response, respectively (Larrivée et al., 2007; Lu et al., 2004; Tu
96 et al., 2015). Whether netrin-1 plays a similar role in guiding vascular development and patterning in the
97 kidney remains unexplored.

98 Here we report that netrin-1 (*Ntn1*) is expressed and secreted by stromal progenitors in the
99 developing kidney. Deletion of *Ntn1* from this population results in hypoplastic kidneys and delayed
100 cessation of nephrogenesis. In correlation with its known role in vascular development, we found that
101 netrin-1 supports proper patterning and maturation of the vasculature during kidney organogenesis.
102 Our findings correlate with those in the accompanying manuscript by **Luo, Gu et al.**, and together we
103 establish a critical role for netrin-1 in mediating proper kidney development through regulation of
104 vascular maturity.

105 **Results**

106 *Ntn1 is expressed and secreted by Foxd1+ stromal progenitors in the developing kidney*

107 While netrin family members including netrin-1 play important roles in other branching
108 organs during development, such as the lung, pancreas, and mammary gland, whether they
109 have a role in kidney development has not been investigated to date(Liu et al., 2004; Srinivasan
110 et al., 2003; Yebra et al., 2003). To begin, we examined the expression pattern of *Ntn1* mRNA in
111 the developing kidney and found that *Ntn1* is expressed by stromal progenitors around the
112 nephron progenitor caps at embryonic day (E)15.5 and, to a lesser extent, in the proximal

113 tubule which is more specifically detected at later postnatal (P2) stages of development (Fig.
114 1A; Fig. S1A). This cellular expression pattern is confirmed by publicly available single cell RNA-
115 seq data of the kidney at E18.5(Combes et al., 2019; England et al., 2020). As early as E11.5,
116 secreted netrin-1 protein was observed surrounding the Six2+ nephron progenitors where the
117 stromal progenitors coalesce (Fig. 1B). At E15.5, netrin-1 was similarly secreted into the area
118 surrounding the nephron progenitor niche (Fig. 1C, arrow). Some protein was diffused into the
119 area below the nephron progenitor niche where ureteric tips lie, potentially acting as a ligand
120 sink to prevent further diffusion (Fig. 1C). The stromal progenitors expressing *Ntn1* give rise to
121 the renal interstitium, mesangial cells, and vascular mural cells, among others, and function in
122 advancing nephron progenitor differentiation(Hatini et al., 1996; Kobayashi et al., 2014;
123 Sequeira-Lopez et al., 2015a), suggesting that netrin-1 signaling may support proper kidney
124 development.

125 *Deletion of Ntn1 from stromal progenitors disrupts normal kidney development*

126 Germline deletion of *Ntn1* was previously shown to result in embryonic lethality by
127 E14.5(Bin et al., 2015). To circumvent this early lethality and address the role of netrin-1 in
128 kidney development, we conditionally deleted *Ntn1* from the Foxd1+ stromal progenitors by
129 using the $Foxd1^{GC}$ allele in combination with a *Ntn1* floxed allele(Bin et al., 2015; Humphreys et
130 al., 2010; Kobayashi et al., 2014). The resulting $Foxd1^{GC/+}$; $Ntn1^{fl/fl}$ mice have very little or no
131 netrin-1 protein present in the interstitial regions surrounding the nephron progenitors,
132 confirming efficient deletion (Fig. 1C). Our initial observations found that $Foxd1^{GC/+}$; $Ntn1^{fl/fl}$
133 mutant animals have hypoplastic kidneys at E15.5 and this phenotype persists postnatally (Fig.
134 1D). Immunostaining of the ureteric tree at E14.5 also revealed qualitative differences in kidney

135 size (Fig. S1B). Measurements of kidney length showed these reductions became most
136 significant after E13.5 (Fig. 1E).

137 As a means of assessing whether *Ntn1* deletion affects either the onset of kidney
138 development or cessation of nephrogenesis, we examined the presence of Six2+ nephron
139 progenitors at the initial branching event (E11.5) and after the cessation of nephrogenesis (P4),
140 which normally occurs around P2-P3 in the mouse(Hartman et al., 2007; Self et al., 2006). At
141 E11.5, we observed no empirical differences in the condensation of Six2+ nephron progenitors
142 around the ureteric buds suggesting kidney development initiated at the same time in *Ntn1*
143 conditional mutants (Fig. 2A). Analysis of nephron progenitor niches at E15.5 revealed no
144 obvious differences in their organization, suggesting normal progression of nephrogenesis (Fig.
145 2B). Strikingly though, at P4, *Foxd1*$^{GC/+}$; *Ntn1*$^{fl/fl}$ kidneys maintained small clusters of Six2+ cells
146 whereas controls had exhausted their Six2+ population as expected (Fig. 2C). Our previous bulk
147 nephron progenitor RNA-seq data as well as recent scRNA-seq data indicate the netrin receptor
148 *Unc5c* is expressed by nephron progenitors(Combes et al., 2019; O'Brien et al., 2018, 2016). *In*
149 *situ* hybridization of *Unc5c* confirmed expression by the nephron progenitors, as well as
150 podocytes and smooth muscle cells of the ureter (Fig. 2D). Due to the nephron progenitor
151 expression, we wondered whether disrupted signaling via netrin-1 to the *Unc5c+* nephron
152 progenitors might account for the smaller kidney size and delay in cessation of nephrogenesis.
153 We assessed the kidney phenotype of whole animal *Unc5c* knockouts(Ackerman et al., 1997)
154 and found no difference in kidney size compared to controls (Fig. 2E). Additionally, the Six2+
155 nephron progenitor niches appear normal, and no other overt phenotypes were observed at

156 any stages examined (Fig 2F). Therefore, the absence of netrin-1 signaling through Unc5c is
157 unlikely to cause the observed hypoplastic phenotype.

158 In developing *Foxd1*$^{GC/+}$; *Ntn1*$^{fl/fl}$ kidneys, the loss of *Ntn1* could affect the number of
159 progenitors in nephron progenitor or ureteric tip niches, leading to hypoplasia. To assess cell
160 numbers, we analyzed kidney sections at multiple timepoints and counted Six2+ nephron
161 progenitors and Ecad+ ureteric tip cells within the niche (Fig. 2G). Apart from a transient
162 difference in tip cell numbers at E13.5, neither population showed any significant differences
163 between *Foxd1*$^{GC/+}$; *Ntn1*$^{fl/fl}$ kidneys and controls when assessed at E13.5, E15.5, and P0 (Fig.
164 2H). Using the same method, we investigated whether the proliferative capacity of niche
165 progenitors was impacted by measuring EdU incorporation into these populations as a measure
166 of cell cycling (Fig. 2G). We found no significant differences in the number of EdU+ cells in
167 either Six2+ or Ecad+ progenitor populations suggesting cell proliferation, at least at the stages
168 analyzed, was not causing the hypoplastic phenotype (Fig. 3C).

169 *Netrin-1 mediates vascular patterning in the developing kidney*

170 Both axons and endothelium respond to guidance cues such as netrin-1 using specific
171 receptors. Unc5b has been shown to mediate angiogenesis (Larrivée et al., 2007; Lu et al., 2004)
172 and *in situ* hybridization at E15.5 shows that *Unc5b* is expressed by the kidney endothelium as
173 well as the ureteric epithelium, although is excluded from the most peripheral ureteric
174 branches(Lindström et al., 2018) (Fig 3A). During kidney development, axonal projections tightly
175 associate and track with the vasculature, forming tight neurovascular bundles (Fig 3B).
176 Therefore, we included both nerves and vessels in our analyses since both have the potential to
177 respond to netrin-1 guidance. To assess overall organization and patterning of these networks,

178 we utilized wholemount immunostaining in combination with light-sheet microscopy to
179 generate 3D visualizations. Control kidneys show the formation of an extensive CD31+
180 endothelial network by E15.5 (Fig. 3C). Tuj1+ axons track closely with the main arterial
181 branches at this stage which form a pattern consistent with those observed by Daniel et
182 al.(Daniel et al., 2018) (Fig 3C, Suppl. Video 1). In contrast, we observed aberrant neuronal and
183 vascular patterning in the *Foxd1*$^{GC/+}$; *Ntn1*$^{fl/fl}$ mutant kidneys (Fig. 3C, Suppl. Video 2). The
184 example shown features looping of the arterial tree within the kidney cortex and ectopic
185 vessels on the kidney surface (arrowheads, Fig. 3C). Tracing of the main CD31+ arterial branches
186 shows that controls form a predictable pattern, as expected, which can be overlayed into 5
187 main branches from a lateral view(Daniel et al., 2018) (Fig. 3D). However, the *Foxd1*$^{GC/+}$; *Ntn1*$^{fl/fl}$
188 kidneys have a breakdown of predictable patterning and overall stochastic patterning (Fig. 3D).
189 Though not a focus of this study, the cortical vasculature around the developing nephron
190 progenitor niches of *Foxd1*$^{GC/+}$; *Ntn1*$^{fl/fl}$ kidneys is also disrupted, featuring disorganized and
191 ectopic vasculature (Fig. S2A). Notably, the presence of Ter119+ erythroid cells indicates that
192 the blood vessels are perfused in both control and *Foxd1*$^{GC/+}$; *Ntn1*$^{fl/fl}$ kidneys at E15.5, although
193 contribution from hemo-vasculogenesis is also possible (Sequeira Lopez et al., 2003)(Fig. S2B).
194 *Ntn3* (netrin-3), a functionally related guidance cue that can engage netrin-1 receptors(Wang et
195 al., 1999), is also expressed, albeit at lower levels, by the stromal progenitors(Combes et al.,
196 2019; England et al., 2020) (Fig S3A). However, we did not observe any neurovascular
197 patterning defects or differences in kidney size in *Ntn3* knockouts or any exacerbation of the
198 *Foxd1*$^{GC/+}$;*Ntn1*$^{fl/fl}$ phenotype when double knockouts (*Foxd1*$^{GC/+}$;*Ntn1*$^{fl/fl}$;*Ntn3*$^{-/-}$) were

199 generated (Fig. S3B,C). Together, these data suggest netrin-1 is the primary netrin guidance cue
200 responsible for the neurovascular patterning defects.

201 As both axons and endothelium can respond to netrin-1 guidance cues, we sought to
202 differentiate the primary responder to stromal-derived netrin-1 signals. Deletion of the *TrkA*
203 receptor for Nerve Growth Factor (NGF) induces apoptosis of peripheral neurons such as those
204 that innervate the kidney(Smeyne et al., 1994). We investigated vascular patterns in the setting
205 of reduced kidney innervation utilizing a *TrkA* knockout allele(Liebl et al., 2000). In *TrkA*
206 knockout kidneys, the vascular pattern was qualitatively normal at E16.5 (Fig. 3E). However,
207 when combined with the *Foxd1*$^{GC/+}$;*Ntn1*$^{fl/fl}$ alleles to generate *Foxd1*$^{GC/+}$;*Ntn1*$^{fl/fl}$;*TrkA*$^{-/-}$ animals,
208 the kidney endothelium still displayed abnormal patterning including looping and ectopic
209 vessels (Fig. 3E). The ectopic and looping vessels were not associated with Tuj1+ axons (Fig. 3E,
210 arrowheads), suggesting the endothelium is the primary responder to netrin-1 guidance cues
211 with the nerves following the vascular pattern, and in particular the smooth muscle coated
212 (alpha-smooth muscle actin, SMA+) endothelium (Fig. 3E). We also wanted to investigate
213 whether *Unc5c* knockout kidneys displayed altered patterning, even though they were not
214 hypoplastic. The neurovascualture appeared largely normal with no ectopic vessels, aberrant
215 looping, or qualitative reductions suggesting Unc5c is not a major receptor for netrin-1 in the
216 kidney or is functionally redundant with another receptor (Fig. S3D).

217 *Vascular smooth muscle cell coverage is reduced in Foxd1*$^{GC/+}$*; Ntn1*$^{fl/fl}$ *kidneys*

218 As the endothelium matures it is covered by a layer of vascular smooth muscle cells
219 (vSMCs). These cells provide support, maintain arterial wall integrity, and can direct innervation
220 through the release of guidance molecules(Brunet et al., 2014; Potente and Mäkinen, 2017). To

221 determine if vSMCs were impacted in *Foxd1*$^{GC/+}$; *Ntn1*$^{fl/fl}$ animals, we investigated SMA coverage
222 of the endothelium in wholemount immunostained kidneys. Despite the lack of predictable
223 patterning, quantification of the CD31+ endothelium in *Foxd1*$^{GC/+}$; *Ntn1*$^{fl/fl}$ kidneys revealed that
224 branching metrics and total vessel length were not significantly affected at E15.5 (Fig S4A, Fig
225 4A). However, the CD31+ endothelium showed qualitative reductions in SMA coverage in
226 *Foxd1*$^{GC/+}$; *Ntn1*$^{fl/fl}$ kidneys compared to controls (Fig. 4B, arrowheads, Suppl. Videos 3,4).
227 Furthermore, *Tuj1*+ axons tracked exclusively with SMA+ vSMCs, representing arteries, and
228 were not found anywhere where endothelium singularly expressed CD31. These data suggest
229 that *Ntn1* loss impacts smooth muscle coverage of the vasculature, which is associated with
230 vessel stabilization and maturity.

231 While vascular patterning defects in *Foxd1*$^{GC/+}$; *Ntn1*$^{fl/fl}$ kidneys are apparent, they are
232 stochastic and highly variable. Since some kidneys appear to have a more significant degree of
233 mis-patterning, they may also display differences in vSMC coverage. However, despite the
234 stochastic patterning differences, quantification of the SMA+ arterial vasculature showed
235 reductions at E15.5 and P0 in *Foxd1*$^{GC/+}$; *Ntn1*$^{fl/fl}$ kidneys (Fig. 4C,D). On average, E15.5 kidneys
236 from *Foxd1*$^{GC/+}$; *Ntn1*$^{fl/fl}$ animals have greater than a 20% reduction in SMA+ arterial metrics
237 including branch number, branch points, and the total length of the vSMC-lined vasculature
238 (Fig. 4D). At P0, reductions in these three vascular parameters were still significant highlighting
239 the persistence of this phenotype throughout development. To determine whether the defects
240 observed in development extended into adulthood, we labelled the vasculature of 2-3 month
241 old *Foxd1*$^{GC/+}$; *Ntn1*$^{fl/fl}$ animals with Evans blue (Fig 4C). Evans blue is a bis-azo dye that
242 fluoresces only while bound to albumin and labels the perfused renal vasculature(Honeycutt

243 and O'Brien, 2021). At two months, quantification of *Foxd1*$^{GC/+}$; *Ntn1*$^{fl/fl}$ kidneys labeled with
244 Evans blue revealed no significant differences in vascular metrics, although all three metrics
245 trended towards a reduction (Fig. 5D). At both 2 and 3 months of age, ectopic vessels were no
246 longer observed and the kidney vasculature has fewer visible defects, although this is difficult
247 to ascertain due to the highly complex vascular network that has formed. However, differences
248 were noted such as meandering, elongated vessels near the cortex (Fig 4C and Fig S4B, red
249 dotted lines) and areas of reduced branching (Fig S4B, yellow arrows). Additionally, we
250 occasionally observed clouds of Evans blue signal outside the vascular network (Fig S4B, white
251 arrowhead) indicating possible leakage and compromise to vessel integrity.

252 *RNA-seq reveals differences in vascular and metabolic programs of Foxd1*$^{GC/+}$*; Ntn1*$^{fl/fl}$ *kidneys*

253 To better understand alterations to transcriptional programs relevant to the vascular
254 immaturity and the hypoplastic phenotype observed in *Foxd1*$^{GC/+}$; *Ntn1*$^{fl/fl}$ animals, we
255 performed bulk RNA-seq on whole kidneys (Table S1). To account for any exacerbated
256 differences due to the loss of one *Foxd1* allele from the *GFP-Cre* insertion, we compared
257 *Foxd1*$^{GC/+}$; *Ntn1*$^{fl/fl}$ mutant kidneys to *Foxd1*$^{GC/+}$; *Ntn1*$^{fl/+}$ heterozygous kidneys. We utilized a
258 cutoff of 1.2-fold as more significant changes may be drowned out due to the bulk analysis.
259 Gene ontology analyses were then performed on up- and downregulated genes to identify
260 biological processes enriched in either category (Tables S2 and S3). In support of our imaging
261 analyses, processes related to the circulatory system and blood vessel development were
262 upregulated in *Foxd1*$^{GC/+}$; *Ntn1*$^{fl/fl}$ kidneys and included genes such as *Notch1*, *Flt1*, *Nrp2*, and
263 *Unc5b* (Fig. 5A, Table S2). Programs related to cell adhesion and cell migration were also
264 upregulated and included genes in the cadherin superfamily and planar cell polarity related

265 genes, respectively (Fig 5A, Table S2). Such pathways may affect the vSMC association with the
266 endothelium in addition to affecting overall kidney development, thus leading to the
267 hypoplastic phenotype. In support of the reduction in vSMC coverage of the endothelium in
268 mutant kidneys, muscle related processes were downregulated and genes in these categories
269 included *Acta2* which encodes for α-SMA and *Myh11* which is a smooth muscle myosin (Fig 5B,
270 Table S3). Additional biological processes downregulated in *Foxd1*$^{GC/+}$; *Ntn1*$^{fl/fl}$ kidneys were
271 related to more general cellular processes such as translation, RNA processing, and glycolysis
272 (Fig 5B). Altogether, these data suggest that in the absence of netrin-1 signaling, the kidney
273 vasculature is more immature (increased angiogenic processes vs arterialization) which may
274 affect metabolic and cellular processes, leading to the hypoplastic phenotype (Fig. 5C).

275 **Discussion**

276 In this study, we demonstrate that stromal progenitor *Ntn1* is necessary for proper
277 patterning and maturation of the kidney arterial network. *Foxd1*$^{GC/+}$; *Ntn1*$^{fl/fl}$ kidneys have
278 visible and quantifiable stochastic vascular patterning defects with reductions in most arterial
279 metrics during embryogenesis and postnatally. These differences in vascular metrics largely
280 resolve in adulthood, although patterning defects are still observed. Furthermore, deletion of
281 *Ntn1* resulted in a delay in the cessation of nephrogenesis and kidney hypoplasia. Altogether,
282 our studies and those in the accompanying manuscript by **Luo, Gu et. al.,** which uncover similar
283 findings, highlight the significance of netrin-1 to proper kidney vascularization and associated
284 development.

285 While we find differences in vascularization in the absence of netrin-1, our analyses
286 relate specifically to the larger arteries and arterioles of the vascular tree. SMA will only label
287 vasculature with sufficient smooth muscle coverage, typically larger arteries and arterioles,
288 missing the capillaries which are primarily covered by NG2+ pericytes. However, **Luo, Gu et. al.**
289 demonstrate a lack of proper NG2+ pericyte localization in early development, suggesting
290 netrin-1 is an important signaling molecule for all vascular mural cells. Additionally, we did not
291 investigate venous formation and patterning during development, primarily owing to a lack of
292 appropriate and agreed-upon markers of the venous vasculature(Daniel et al., 2018). Veins are
293 also covered with significantly fewer SMCs due to a decreased need to regulate pressure and
294 tone[38]. This makes SMA an unreliable venous marker at lower magnifications, such as those
295 used by light-sheet microscopy to image the vasculature. Therefore, additional studies are
296 necessary to determine to what extent the entire vascular plexus is disrupted in *Foxd1*$^{GC/+}$;
297 *Ntn1*$^{fl/fl}$ kidneys.

298 Vascular patterning and maturity are both disrupted in the *Foxd1*$^{GC/+}$; *Ntn1*$^{fl/fl}$ kidneys in
299 our study. **Luo, Gu et. al.** further define the maturity phenotype as being associated with the
300 loss of Klf4 and accumulation of mural cells on the surface of the kidneys. We did not observe
301 any obvious accumulation of mural cells at E15.5 or later stages, and whether Klf4 is associated
302 with the phenotype in our studies is unknown. We did not find a difference in *Klf4* expression in
303 our E15.5 RNA-seq, although this is 2 days later than the RNA-seq performed by **Luo, Gu et. al.**
304 and Klf4 levels may have normalized by this time. Therefore, the observed maturation
305 phenotypes may initiate at the earliest stages of arterialization, around E13.5, and prior to our
306 analysis at E15.5(Daniel et al., 2018). The timing of the phenotype could explain the differences

307 between our study and that of **Luo, Gu et. al.,** highlighting the complementary nature of our
308 analyses. VSMCs *in vitro* express netrin receptors such as Neogenin (*Neo1*) and Unc5b and
309 signaling through these receptors supports endothelial vSMC coverage(Lejmi et al., 2014, 2008).
310 As such, deletion of *Ntn1* from the stroma may ultimately impact SMC maturation or
311 recruitment in the kidney and, in turn, affect vascular patterning. This is similar to the findings
312 of Hurtado et al. who showed that Pbx1-mediates mural cell maturation ultimately influencing
313 proper vascular patterning within the developing kidney(Hurtado et al., 2015). Alternatively,
314 patterning of the endothelium may influence vascular maturation. Deletion of *Unc5b* from the
315 kidney endothelium and the assessment of vascular patterning and maturity would potentially
316 help sort out if the patterning defects we observed are independent of vSMC coverage. The lack
317 of significant phenotypes in the *Unc5c* knockouts suggest it is either not a major receptor for
318 netrin-1 in the kidney, or it is functionally redundant. Considering netrin-1 can signal through a
319 large number of receptors, including integrins, and display receptor independent cross-
320 repressive activities with LRIG proteins, uncovering the receptor(s) and downstream signaling
321 mechanisms of netrin-1 in the kidney may prove challenging (Abdullah et al., 2021; Abraira et
322 al., 2008; Stanco et al., 2009; Sun et al., 2011; Yebra et al., 2003).

323 The kidney hypoplasia observed in our *Foxd1*$^{GC/+}$*; Ntn1*$^{fl/fl}$ mutants may be linked to the
324 relative vascular immaturity we observed. This could perturb metabolic processes within the
325 kidney leading to downregulation of the glycolysis pathways and associated genes in our RNA-
326 seq data, and ultimately affect proper kidney growth and prolong the nephrogenic period(Liu et
327 al., 2017). Alternatively, a mechanism independent of the vasculature may perturb proper
328 kidney development. Altered interactions between netrin-1 and Bmp4 could lead to the

329 hypoplastic phenotype. Bmp4 is a negative regulator of ureteric branching through its
330 modulation of Gdnf signaling(Miyazaki et al., 2000). Dysregulation of Gdnf signaling can result
331 in hypoplasia and agenesis at the extreme(Moore et al., 1996; Pichel et al., 1996; Sánchez et al.,
332 1996). Netrin-1 suppresses Bmp4 signaling *in vitro,* and netrin-1 mediated modulation of Bmp
333 signaling within the kidney could help balance Gdnf signaling(Abdullah et al., 2021). It is
334 possible that loss of *Ntn1* results in increases in Bmp4 and a subsequent reduction in Gdnf
335 activity, leading to renal hypoplasia. Our RNA-seq analyses did not reveal any significant
336 perturbations to *Bmp4* or *Gdnf* levels, although assessing an earlier timepoint when the
337 hypoplasia is initiated may be more informative and help sort out the cause of the hypoplastic
338 phenotype.

339 Whether the development of a kidney with abnormal vascular patterns affects
340 physiological function remains unknown and will be the focus of future studies. *Foxd1*$^{GC/+}$;
341 *Ntn1*$^{fl/fl}$ animals do live into adulthood, with no significant kidney or health phenotypes.
342 However, if the smaller vascular beds in important functional regions of the nephron such as
343 the glomerulus and tubules are organized properly, then physiological function may be largely
344 unperturbed. However, injury, disease, or aging may exacerbate or induce changes in
345 physiological function in these animals regardless. Understanding whether precise vascular
346 patterning is critical to function, both in health and under physiological stress, will help inform
347 efforts to vascularize tissues for functional transplant.

348 As the kidney lacks regenerative mechanisms, *de novo* kidney engineering and *in situ*
349 repair using *in vitro* generated nephrons or iPSC-derived renal organoids are considered
350 attractive therapeutic possibilities(Morizane et al., 2015; Taguchi et al., 2014; Takasato et al.,

351 2015; Wu et al., 2018). Unfortunately, neither treatment is currently approaching clinical
352 relevance(Bantounas et al., 2018). With current protocols, renal organoids form basic nephron
353 structures but eventually become necrotic from a deficit of oxygen and nutrients since
354 functional endothelium is not present(Grebenyuk and Ranga, 2019). Interestingly, cells
355 expressing the pan-endothelial marker CD31 occur *de novo* in organoids, but without perfusion
356 they do not form connected, functional networks, resulting in a lack of proper lumenization,
357 flow, and patterning and their eventual regression(Homan et al., 2019; Ryan et al., 2021;
358 Taguchi et al., 2014; Wu et al., 2018). Additionally, the vessels would need to obtain
359 appropriate mural cell coverage to support function. Therefore, studies such as ours and those
360 of **Luo, Gu et. al.** provide critical insights into how the renal vasculature is patterned, matures,
361 and contributes to kidney development and will help guide kidney engineering strategies.

362 **Material and methods**

363 *Animals*

364 All animal studies were approved by the Office of Animal Care and Use at the University
365 of North Carolina at Chapel Hill and the UNC Institutional Animal Care and Use Committee
366 (IACUC). Procedures were performed under IACUC-approved protocols for mice (16-276.0, 19-
367 183.0, 22-136). Animal husbandry is performed by UNC's Division of Comparative Medicine
368 (DCM). All animals in this study were kept in environmental conditions consisting of
369 temperatures between 68-74˚F, with humidity ranges of 30-70%. No more than five adult
370 animals were housed per cage, and all cages were provided a 12-hour light/dark cycle. Animals
371 are fed LabDiet PicoLab Select Rodent 50 IF/6F (Catalog #, 5V5R). Timed matings were set up
372 and plugs were ascertained by visual and probed inspection. The presence of a plug was

373 considered 0.5 days gestation. The day of birth (E19.5) was considered postnatal day 0 (P0),
374 pups born before or after E19.5 were not utilized in these studies.

375 All mouse lines are maintained on the C57Bl6/J background (Jackson Labs, Strain
376 #000664). Details of genetically edited mouse lines utilized are as follows: *Foxd1*$^{GC/+}$ (Strain
377 #012463)(Humphreys et al., 2010; Kobayashi et al., 2014) and *Ntn1*$^{fl/fl}$ (Strain #028038)(Bin et
378 al., 2015) mice were purchased from Jackson Labs, *TrkA* knockout mice(Liebl et al., 2000) were
379 a gift from Lino Tessarollo at the NIH National Cancer Institute Center for Cancer Research, and
380 *Unc5c* knockout mice(Ackerman et al., 1997) were a gift from Susan Ackerman at the University
381 of California, San Diego. *Foxd1*$^{GC/+}$*; Ntn1*$^{fl/fl}$ mice were generated by crossing Cre-expressing
382 *Foxd1*$^{GC/+}$*; Ntn1*$^{f/+}$ to *Ntn1*$^{fl/fl}$ mice unless otherwise noted. Controls were either *Ntn1*$^{c/c}$ or
383 *Foxd1*$^{GC/+}$*; Ntn1*$^{fl/+}$ as we did not find any qualitative or quantitative differences between
384 genotypes for any of the analyses.

385 *Ntn3* knockout mice were generated by the UNC Animal Models Core using
386 CRISPR/Cas9-mediated genome editing. Guide RNAs *Ntn3*-gRNA1 (CGAGGAATCGCAGACGCGAT,
387 Exon 1, chr17:24208777-24208796) and *Ntn3*-gRNA2 (GAAAGCGTGTCCACGAGCCG, Intron 5,
388 chr17:24206891-24206910) were designed to delete the majority of the *Ntn3* coding region
389 spanning Exons 1-6. Guide RNAs were generated within our lab and provided to the animal
390 models core at estimated concentrations of 500ng/µl and 450ng/µl, respectively. Guide RNAs
391 were prepared as in O'Brien et al.(O'Brien et al., 2018). Recombinant Cas9 protein was
392 expressed and purified by the UNC Protein Expression Core using a plasmid provided by the
393 Animal Models Core. Two hundred and ten fertilized embryos (zygotes) were harvested from 9
394 super-ovulated *Ntn1*$^{fl/fl}$ females crossed to *Foxd1*$^{GC/+}$*; Ntn1*$^{fl/fl}$ males. Zygotes were

395 electroporated with two different reagent concentrations diluted in OptiMEM medium (Gibco)
396 and then implanted in pseudo-pregnant recipient females. Mix 1: 1.2 µM Cas9 protein, 47 ng/µl
397 each guide RNA. 102 embryos electroporated; 85 embryos implanted in 4 B6D2F1 recipients.
398 Mix2: 400 nM Cas9 protein, 25 ng/µl each guide RNA. 108 embryos electroporated; 95 embryos
399 implanted in 4 B6D2F1 recipients. Of the resulting pups, one male containing the correct
400 deletion as confirmed by Sanger sequencing over the deletion site was used as the founder.
401 Brain and kidney tissue was harvested, and qPCR performed to confirm the loss of *Ntn3*
402 transcripts in knockout animals.

403 Genotyping primers utilized in this study: *Ntn1* F: GGCAGTGAATGTGTTTCCGTT, *Ntn1* R:
404 ATCGCGGGATAGTGGGTTTC; *Foxd1* WT F: CTCCTCCGTGTCCTCGTC, *Foxd1* Mut F:
405 GGGAGGATTGGGAAGACAAT, *Foxd1* Common R: TCTGGTCCAAGAATCCGAAG; *Ntn3* Internal
406 (WT) F: GGCCTGTGGTCTGGTTACAG, *Ntn3* Internal (WT) R: TAGCCTGGGGACTTCTGACC, *Ntn3*
407 External (deletion) F: CACCTCCCAGCAGCAAGTAAC, *Ntn3* External (deletion) R:
408 ACGCAGAGTAGCGGACTAGG; *TrkA* 1: TGTACGGCCATAGATAAGCAT, *TrkA* 2:
409 TGCATAACTGTGTATTTCAC, *TrkA* 3: CGCCTTCTTGACGAGTTCTTCTG; *Unc5c* WT F:
410 CACTCTATGGAAATGGCTGAAT, *Unc5c* WT R: GTCCTCCAATCCAAGAACTG, *Unc5c* Mut F:
411 CAGGAGAAGATACATTTAACCAC, *Unc5c* Mut R: GACAGAAGAGCATAGCATTCAC

412 *Kidney size measurements*

413 Kidney length measurements were performed using FIJI software to analyze images
414 taken at 2x magnification on a Leica dissecting scope. Standardization and calibration of FIJI
415 measurements were performed using a 1µm-1mm micrometer taken at the same
416 magnification.

417 *In situ hybridization*

418 *In situ* hybridizations were performed on wildtype cryosectioned E15.5 and P2 Swiss
419 Webster (SW, Taconic) kidneys using the "Section In Situ Hybridization (SISH) on kidney
420 sections" protocol (Krautzberger and Guo; McMahon Lab;
421 https://www.gudmap.org/chaise/record/#2/Protocol:Protocol/RID=N-H9AC) on GUDMAP
422 (www.gudmap.org). Digoxygenin (DIG) labeled probes were generated following the
423 "Digoxigenin-labelled Riboprobe Synthesis from a PCR-generated DNA templates" protocol
424 found on GUDMAP (Little Group, GUDMAP Consortium). Primers utilized for probes are as
425 follows: *Ntn1* F:CTTCCTCACCGACCTCAATAAC, *Ntn1* (SP6) R:
426 GCGATTTAGGTGACACTATAGTTGTGCCTACAGTCACACACC; *Ntn3* F:GGCACGCTCTCCGCTGCA,
427 *Ntn3* (T7) R:TAATACGACTCACTATAGGGAGTGGCTGAGTAGGAGTA; *Unc5c*
428 F:ATGAGGAAAGGTCTGAGGGCGACAG, *Unc5c* (T7)
429 R:TAATACGACTCACTATAGGGAGAGAGTTGAAGGTACCAA; *Unc5b* F:TCAAGTGTAATGGCGAGTG,
430 *Unc5b* (T7) R:TAATACGACTCACTATAGGGGCCTCCATTCACATAGACGA

431 *Section immunostaining*

432 For all samples, kidneys were harvested at the necessary time point. Tissue was then
433 fixed in 4% paraformaldehyde (PFA) in 1 x PBS for 15-30 minutes (embryonic/postnatal) to 24
434 hours (adult). Kidneys were washed 2x in PBS and stored for up to two weeks before
435 processing. Samples were incubated in 30% sucrose in PBS overnight at 4 ^{o}C. Tissue was
436 embedded in OCT media, frozen with 100% EtOH and dry ice, and stored at -80 ^{o}C for up to two
437 years. Frozen tissue was sectioned at 10-12µm. Sections were air-dried at room temperature
438 (RT) for a minimum of 10 minutes. Samples were then incubated in 1x PBS for 5 minutes to

439 remove OCT media. Next, sections were placed in blocking buffer (PBS with 3% BSA, 1% donkey
440 serum, and 0.25% Triton x-100) for 20 minutes at RT. The blocking buffer was removed, then
441 sections were incubated with primary antibodies in the blocking buffer for 1 hour at RT.
442 Sections were then rinsed 3x in wash buffer (PBS with 0.1% Triton x-100). Next, sections were
443 incubated with appropriate Alexa Fluor conjugated secondary antibodies at 1:1000 (Invitrogen)
444 in blocking buffer for 20 minutes. Sections were then rinsed 3x in wash buffer and mounted
445 with Prolong Gold with DAPI (Invitrogen). Antibodies utilized and their dilution are listed in
446 Table S4.

447 *Quantification of proliferation*

448 Mice were injected intraperitoneally with 1.25 mg of EdU (10mg/ml) 1.5 hours before
449 euthanasia and tissue collection. For analysis of proliferation, the following procedure was
450 used. The tissue was fixed, then sectioned and stained as described previously in this report.
451 The Click-It EdU kit was utilized to detect EdU positive cells. Images were then collected on a
452 Zeiss 880 confocal using a 40x oil objective. The whole kidney images were created through
453 automated tiling of the tissue section using Zen Black software. Reconstruction of the images
454 into a single image was performed using Imaris stitcher (Bitplane). For proliferation counts, a
455 minimum of 10 nephrogenic caps were counted per section for each genotype and age.
456 Quantitation of proliferation for nephron progenitors was determined as the number of cells
457 colocalized for both EdU and Six2 divided by the total number of Six2+ cells. Ureteric bud (UB)
458 tip niches were defined as the Ecad+ cells within the UB but above the ventral end of the
459 nephrogenic cap. Quantitation for UB proliferation was determined as the number of cells

460 within the UB niche colocalized with Ecad and EdU divided by the total number of Ecad+ cells
461 within the UB niche.

462 *Wholemount immunostaining*

463 The wholemount immunostaining protocol was adapted from Jafree et al.(Jafree et al.,
464 2019) and Renier et al.(Renier et al., 2014). All following steps are performed with rocking
465 unless otherwise noted. Samples are collected and fixed in 4% PFA for 15-30 minutes
466 (embryonic/postnatal). Tissue is washed with rocking 2x for 20 minutes at RT. Samples are then
467 dehydrated in an increasing MeOH/H_2O series of 25%, 50%, 75%, and 100% for 30 minutes or 1
468 hour, depending on tissue size. Next, tissue is bleached overnight in 5% H_2O_2 (from 30% stock)
469 in 100% MeOH. Samples are then rehydrated following a reverse MeOH/H_2O series (100%, 75%,
470 50%, 25%, PBS) for 30 minutes or 1 hour, depending on tissue size. Tissue is then permeabilized
471 overnight at 4 ^{o}C in PBS with 0.2% Triton x-100, 2.3% glycine, and 20% DMSO. The
472 permeabilization solution is removed, and blocking buffer (PBS with 0.2% triton x-100, 6%
473 donkey serum, and 10% DMSO) is added; the tissue is then incubated for one day at RT. The
474 blocking buffer is then removed, and primary antibody in staining solution (PBS with 0.2%
475 Tween-20, 0.1% heparin [from 10mg/ml stock], 3% donkey serum, and 5% DMSO) is added to
476 samples, which are then incubated for three days at 4°C, followed by washing 4-6x for 1 hour at
477 RT in wash buffer (PBS with 0.2% Tween-20 and 0.1% heparin [from 10mg/ml stock]). The
478 appropriate Alexa fluor labeled secondary antibody in staining solution is then added (1:250)
479 and incubated overnight at 4°C. Samples are washed 4-6x for 1 hour at RT in wash buffer.
480 Samples are then immediately moved to clearing or stored at 4°C in 1x PBS, protected from

481 light until ready to proceed to clearing. Antibodies utilized and their dilution are listed in Table
482 S4.

483 *Evans blue*

484 The full protocol for Evans blue dye is from Honeycutt and O'Brien(Honeycutt and
485 O'Brien, 2021) and is described here briefly. Animals are anesthetized to a surgical plane under
486 isoflurane. Next, the chest cavity and peritoneum are cut to expose the diaphragm. 2% Evans
487 blue dye in 0.9% $NaCl/H_2O$ at 3 µl/g of body weight is injected into the left ventricle with either
488 a 25g needle or 31g insulin syringe. The dye is allowed to circulate until the exposed areas
489 (paws, tail, chin) turn blue, roughly 2-5 minutes. The animal is subsequently euthanized, and
490 kidney is collected, rinsed briefly in PBS several times to remove excess dye, then fixed in 4%
491 PFA for 24 hours at 4°C. Samples are washed in PBS and stored at 4°C until clearing.

492 *Tissue clearing and imaging*

493 This protocol was adapted from the iDISCO method of tissue clearing(Renier et al.,
494 2014). First, embryonic and small samples are placed into agarose blocks (1% agarose in tris-
495 acetate-EDTA [TAE]). Adult kidneys are not embedded. All following steps are performed with
496 rocking unless otherwise noted. These blocks or adult kidneys are dehydrated in an increasing
497 $MeOH/H_2O$ series of 25%, 50%, 75%, and 100% for 30 minutes or 1 hour at RT, depending on
498 tissue size. Samples are then incubated in 66% dichloromethane (DCM) / 33% MeOH for 3
499 hours at RT. Next, two rounds of incubation with 100% DCM at RT are performed. DCM is
500 removed, and 100% dibenzyl ether (DBE) is added. Samples are incubated, with no rocking,
501 until clear (1 – 24 hours) and stored indefinitely in 100% DBE at either RT or 4 ^{o}C, protected
502 from light, until ready to proceed to imaging. Light-sheet imaging of whole kidneys was

503 performed using a LaVision UltraMicroscope II (LaVision BioTec). 3D reconstruction of images
504 and vascular network quantification was conducted using Imaris imaging software (Bitplane).

505 *Quantification of wholemount 3D vasculature*

506 To conduct quantification of renal vasculature within Imaris, a surface of the 3D image
507 was first created to digitally render the vasculature. Next, a binary mask of the rendered
508 surface was created using the “Mask channel" function with “Constant inside/outside” settings
509 for voxel intensity set to 0 outside and 100 inside. This was necessary to render the vasculature
510 effectively solid, so that the filament tracer module within Imaris could be implemented to
511 develop wireframes for statistical analysis. Kidneys were batched with similar parameters per
512 age group. Then supervised automatic tracing was performed to ensure that automatically
513 generated paths were not duplicated, or artifacts inaccurately rendered as vasculature. As both
514 kidneys from the same animal have highly similar statistical values, with little deviation when
515 averaged, for most studies, only one kidney per animal was needed for quantification. This
516 method was used to quantify renal arterial trees for Evans blue in adults and SMA and CD31
517 staining in the embryonic and neonatal kidneys. Cortical arterioles and vascular beds were
518 excluded from analysis.

519 For graphical display of vascular patterning and imaging that were not quantified, a
520 surface was created for the desired channel. This surface was then masked using the same
521 procedure, but “Constant inside/outside” settings for voxel intensity were set to 0 outside with
522 the inside setting left unchecked.

523 *RNA-seq*

524 Whole kidneys were collected at E15.5 from 3 separate *Ntn1*$^{fl/fl}$ x *Foxd1*$^{GC/+}$;*Ntn1*$^{fl/+}$
525 crosses. Three kidneys were collected of each genotype: *Foxd1*$^{GC/+}$;*Ntn1*$^{fl/+}$ (heterozygous),
526 *Foxd1*$^{GC/+}$;*Ntn1*$^{fl/fl}$ (homozygous), and *Ntn1*$^{fl/fl}$ (wildtype). Kidneys were placed in RNAlater
527 (Thermo Fisher) until all samples were collected. RNA was extracted with TRIzol (Invitrogen).
528 RNA was sent to Cancer Genetics Inc (Morrisville, NC) for sequencing and data processing. RNA
529 samples were converted to sequencing libraries using the TruSeq Stranded mRNA kit (Illumina
530 Cat. #20020595). Resulting libraries were assessed for quality via analysis on a 2100 Bioanalyzer
531 (Agilent Technologies) and quantitated by qPCR (KAPA Library Quantification; Roche: KK4824,
532 Cat# 07960140001). Normalized and pooled libraries were sequenced on the Illumina Nextseq
533 550 system. Alignment and analysis were performed following a modified Tuxedo workflow.
534 Briefly, alignment was done with STAR aligner followed by cufflinks/cuffmerge for assembled
535 transcripts. FPKM was calculated with CuffDif and analyzed with the R package. Heterozygous
536 samples were used as a control and comparison to the homozygous samples to account for any
537 effects of the hemizygous *Foxd1* allele due to the knock-in of GFP-Cre into the *Foxd1* locus. A
538 count of 5 FPKM was considered minimum criteria for expression in the whole kidney RNA-seq,
539 genes with less than this FPKM (unless downregulated compared to the reference) were
540 excluded from gene expression analyses. Up- and downregulated gene lists were pasted into
541 the Database for Annotation, Visualization and Integrated Discovery (DAVID) to obtain Gene
542 Ontology information and enrichment.
543

544 **Acknowledgments**

We thank members of the O'Brien lab for technical help and critical discussions, Dr. Pablo Ariel, director of the UNC Microscopy Services Laboratory, for assistance with light-sheet imaging and Imaris rendering/analysis, Dr. Robert Currin (retired) of the UNC Hooker Imaging Core for confocal microscopy imaging assistance, and Dr. Dale Cowley, director of the UNC Animal Models Core, for help with *Ntn3* knockout mouse generation. We thank Drs. Lino Tessarollo (NCI) and Susan Ackerman (UCSD) for their kind gifts of *TrkA* and *Unc5c* knockout mice, respectively.

Author Contributions

LLO conceived and designed the project, performed experiments, analyzed data, and helped write the manuscript. SEH helped design the experiments, performed experiments, analyzed data, and wrote the manuscript. P-EYN, DMH, YX, and SLC performed experiments and analyzed data.

Competing Interests

The authors have nothing to declare and no competing interests, relevant affiliations, financial involvement, or financial conflicts with any entities or organizations that may have financial interests in the research, subject matter, or materials in this manuscript apart from those disclosed.

Funding

565 This work was supported by NIH R01DK121014 (LLO), 5T32HL069768 (SEH), and the
566 Ross and Charlotte Johnson Family Dissertation Fellowship (SEH). The UNC Animal Models Core,
567 the Microscopy Services Laboratory, and UNC Hooker Imaging Core Facility are supported in
568 part by the P30 CA016086 Cancer Center Core Support Grant to the UNC Lineberger
569 Comprehensive Cancer Center.

570

571 **References**

572

573 Abdullah, A., Herdenberg, C., Hedman, H., 2021. Netrin-1 functions as a suppressor of bone
574 morphogenetic protein (BMP) signaling. Sci Rep 11, 8585. https://doi.org/10.1038/s41598-021-
575 87949-7
576 Abraira, V.E., del Rio, T., Tucker, A.F., Slonimsky, J., Keirnes, H.L., Goodrich, L.V., 2008. Cross-repressive
577 interactions between Lrig3 and netrin 1 shape the architecture of the inner ear. Development
578 135, 4091–4099. https://doi.org/10.1242/dev.029330
579 Ackerman, S.L., Kozak, L.P., Przyborski, S.A., Rund, L.A., Boyer, B.B., Knowles, B.B., 1997. The mouse
580 rostral cerebellar malformation gene encodes an UNC-5-like protein. Nature 386, 838–842.
581 https://doi.org/10.1038/386838a0
582 Adams, R.H., Eichmann, A., 2010. Axon Guidance Molecules in Vascular Patterning. Cold Spring Harb
583 Perspect Biol 2, a001875. https://doi.org/10.1101/cshperspect.a001875
584 Bantounas, I., Ranjzad, P., Tengku, F., Silajdžić, E., Forster, D., Asselin, M.-C., Lewis, P., Lennon, R.,
585 Plagge, A., Wang, Q., Woolf, A.S., Kimber, S.J., 2018. Generation of Functioning Nephrons by
586 Implanting Human Pluripotent Stem Cell-Derived Kidney Progenitors. Stem Cell Reports 10, 766–
587 779. https://doi.org/10.1016/j.stemcr.2018.01.008
588 Barry, D.M., McMillan, E.A., Kunar, B., Lis, R., Zhang, T., Lu, T., Daniel, E., Yokoyama, M., Gomez-Salinero,
589 J.M., Sureshbabu, A., Cleaver, O., Di Lorenzo, A., Choi, M.E., Xiang, J., Redmond, D., Rabbany,
590 S.Y., Muthukumar, T., Rafii, S., 2019. Molecular determinants of nephron vascular specialization
591 in the kidney. Nat Commun 10, 5705. https://doi.org/10.1038/s41467-019-12872-5
592 Bin, J.M., Han, D., Lai Wing Sun, K., Croteau, L.-P., Dumontier, E., Cloutier, J.-F., Kania, A., Kennedy, T.E.,
593 2015. Complete Loss of Netrin-1 Results in Embryonic Lethality and Severe Axon Guidance
594 Defects without Increased Neural Cell Death. Cell Rep 12, 1099–1106.
595 https://doi.org/10.1016/j.celrep.2015.07.028
596 Blei, F., Bittman, M.E., 2016. Congenital vascular anomalies: current perspectives on diagnosis,
597 classification, and management. JVD 4, 23–37. https://doi.org/10.2147/JVD.S63244
598 Brunet, I., Gordon, E., Han, J., Cristofaro, B., Broqueres-You, D., Liu, C., Bouvrée, K., Zhang, J., del Toro,
599 R., Mathivet, T., Larrivée, B., Jagu, J., Pibouin-Fragner, L., Pardanaud, L., Machado, M.J.C.,
600 Kennedy, T.E., Zhuang, Z., Simons, M., Levy, B.I., Tessier-Lavigne, M., Grenz, A., Eltzschig, H.,
601 Eichmann, A., 2014. Netrin-1 controls sympathetic arterial innervation. J Clin Invest 124, 3230–
602 3240. https://doi.org/10.1172/JCI75181
603 Combes, A.N., Phipson, B., Lawlor, K.T., Dorison, A., Patrick, R., Zappia, L., Harvey, R.P., Oshlack, A.,
604 Little, M.H., 2019. Single cell analysis of the developing mouse kidney provides deeper insight

605 into marker gene expression and ligand-receptor crosstalk. Development 146, dev178673.
606 https://doi.org/10.1242/dev.178673
607 Daniel, E., Azizoglu, D.B., Ryan, A.R., Walji, T.A., Chaney, C.P., Sutton, G.I., Carroll, T.J., Marciano, D.K.,
608 Cleaver, O., 2018. Spatiotemporal heterogeneity and patterning of developing renal blood
609 vessels. Angiogenesis 21, 617–634. https://doi.org/10.1007/s10456-018-9612-y
610 England, A.R., Chaney, C.P., Das, A., Patel, M., Malewska, A., Armendariz, D., Hon, G.C., Strand, D.W.,
611 Drake, K.A., Carroll, T.J., 2020. Identification and characterization of cellular heterogeneity
612 within the developing renal interstitium. Development 147, dev190108.
613 https://doi.org/10.1242/dev.190108
614 Gerety, S.S., Wang, H.U., Chen, Z.F., Anderson, D.J., 1999. Symmetrical mutant phenotypes of the
615 receptor EphB4 and its specific transmembrane ligand ephrin-B2 in cardiovascular development.
616 Mol Cell 4, 403–414. https://doi.org/10.1016/s1097-2765(00)80342-1
617 Gitler, A.D., Lu, M.M., Epstein, J.A., 2004. PlexinD1 and semaphorin signaling are required in endothelial
618 cells for cardiovascular development. Dev Cell 7, 107–116.
619 https://doi.org/10.1016/j.devcel.2004.06.002
620 Gomez, R.A., Lynch, K.R., Sturgill, B.C., Elwood, J.P., Chevalier, R.L., Carey, R.M., Peach, M.J., 1989.
621 Distribution of renin mRNA and its protein in the developing kidney. Am J Physiol 257, F850-858.
622 https://doi.org/10.1152/ajprenal.1989.257.5.F850
623 Grebenyuk, S., Ranga, A., 2019. Engineering Organoid Vascularization. Front Bioeng Biotechnol 7, 39.
624 https://doi.org/10.3389/fbioe.2019.00039
625 Gu, C., Rodriguez, E.R., Reimert, D.V., Shu, T., Fritzsch, B., Richards, L.J., Kolodkin, A.L., Ginty, D.D., 2003.
626 Neuropilin-1 conveys semaphorin and VEGF signaling during neural and cardiovascular
627 development. Dev Cell 5, 45–57. https://doi.org/10.1016/s1534-5807(03)00169-2
628 Gu, C., Yoshida, Y., Livet, J., Reimert, D.V., Mann, F., Merte, J., Henderson, C.E., Jessell, T.M., Kolodkin,
629 A.L., Ginty, D.D., 2005. Semaphorin 3E and plexin-D1 control vascular pattern independently of
630 neuropilins. Science 307, 265–268. https://doi.org/10.1126/science.1105416
631 Hartman, H.A., Lai, H.L., Patterson, L.T., 2007. Cessation of Renal Morphogenesis in Mice. Dev Biol 310,
632 379–387. https://doi.org/10.1016/j.ydbio.2007.08.021
633 Hatini, V., Huh, S.O., Herzlinger, D., Soares, V.C., Lai, E., 1996. Essential role of stromal mesenchyme in
634 kidney morphogenesis revealed by targeted disruption of Winged Helix transcription factor BF-
635 2. Genes Dev 10, 1467–1478. https://doi.org/10.1101/gad.10.12.1467
636 Heimann, H., Damato, B., 2010. Congenital vascular malformations of the retina and choroid. Eye 24,
637 459–467. https://doi.org/10.1038/eye.2009.310
638 Homan, K.A., Gupta, N., Kroll, K.T., Kolesky, D.B., Skylar-Scott, M., Miyoshi, T., Mau, D., Valerius, M.T.,
639 Ferrante, T., Bonventre, J.V., Lewis, J.A., Morizane, R., 2019. Flow-enhanced vascularization and
640 maturation of kidney organoids in vitro. Nat Methods 16, 255–262.
641 https://doi.org/10.1038/s41592-019-0325-y
642 Honeycutt, S.E., O'Brien, L.L., 2021. Injection of Evans blue dye to fluorescently label and image intact
643 vasculature. Biotechniques 70, 181–185. https://doi.org/10.2144/btn-2020-0152
644 Humphreys, B.D., Lin, S.-L., Kobayashi, A., Hudson, T.E., Nowlin, B.T., Bonventre, J.V., Valerius, M.T.,
645 McMahon, A.P., Duffield, J.S., 2010. Fate tracing reveals the pericyte and not epithelial origin of
646 myofibroblasts in kidney fibrosis. Am J Pathol 176, 85–97.
647 https://doi.org/10.2353/ajpath.2010.090517
648 Hurtado, R., Zewdu, R., Mtui, J., Liang, C., Aho, R., Kurylo, C., Selleri, L., Herzlinger, D., 2015. Pbx1-
649 dependent control of VMC differentiation kinetics underlies gross renal vascular patterning.
650 Development 142, 2653–2664. https://doi.org/10.1242/dev.124776
651 Jafree, D.J., Moulding, D., Kolatsi-Joannou, M., Perretta Tejedor, N., Price, K.L., Milmoe, N.J., Walsh, C.L.,
652 Correra, R.M., Winyard, P.J., Harris, P.C., Ruhrberg, C., Walker-Samuel, S., Riley, P.R., Woolf, A.S.,

653 Scambler, P.J., Long, D.A., 2019. Spatiotemporal dynamics and heterogeneity of renal lymphatics
654 in mammalian development and cystic kidney disease. Elife 8, e48183.
655 https://doi.org/10.7554/eLife.48183
656 Jones, C.A., London, N.R., Chen, H., Park, K.W., Sauvaget, D., Stockton, R.A., Wythe, J.D., Suh, W.,
657 Larrieu-Lahargue, F., Mukouyama, Y.-S., Lindblom, P., Seth, P., Frias, A., Nishiya, N., Ginsberg,
658 M.H., Gerhardt, H., Zhang, K., Li, D.Y., 2008. Robo4 stabilizes the vascular network by inhibiting
659 pathologic angiogenesis and endothelial hyperpermeability. Nat Med 14, 448–453.
660 https://doi.org/10.1038/nm1742
661 Kennedy, T.E., Serafini, T., de la Torre, JoséR., Tessier-Lavigne, M., 1994. Netrins are diffusible
662 chemotropic factors for commissural axons in the embryonic spinal cord. Cell 78, 425–435.
663 https://doi.org/10.1016/0092-8674(94)90421-9
664 Kobayashi, A., Mugford, J.W., Krautzberger, A.M., Naiman, N., Liao, J., McMahon, A.P., 2014.
665 Identification of a multipotent self-renewing stromal progenitor population during mammalian
666 kidney organogenesis. Stem Cell Reports 3, 650–662.
667 https://doi.org/10.1016/j.stemcr.2014.08.008
668 Larrivée, B., Freitas, C., Trombe, M., Lv, X., DeLafarge, B., Yuan, L., Bouvrée, K., Bréant, C., Toro, R.D.,
669 Bréchot, N., Germain, S., Bono, F., Dol, F., Claes, F., Fischer, C., Autiero, M., Thomas, J.-L.,
670 Carmeliet, P., Tessier-Lavigne, M., Eichmann, A., 2007. Activation of the UNC5B receptor by
671 Netrin-1 inhibits sprouting angiogenesis. Genes Dev. 21, 2433–2447.
672 https://doi.org/10.1101/gad.437807
673 Lejmi, E., Bouras, I., Camelo, S., Roumieux, M., Minet, N., Leré-Déan, C., Merkulova-Rainon, T., Autret,
674 G., Vayssettes, C., Clement, O., Plouët, J., Leconte, L., 2014. Netrin-4 promotes mural cell
675 adhesion and recruitment to endothelial cells. Vasc Cell 6, 1. https://doi.org/10.1186/2045-
676 824X-6-1
677 Lejmi, E., Leconte, L., Pédron-Mazoyer, S., Ropert, S., Raoul, W., Lavalette, S., Bouras, I., Feron, J.-G.,
678 Maitre-Boube, M., Assayag, F., Feumi, C., Alemany, M., Jie, T.X., Merkulova, T., Poupon, M.-F.,
679 Ruchoux, M.-M., Tobelem, G., Sennlaub, F., Plouët, J., 2008. Netrin-4 inhibits angiogenesis via
680 binding to neogenin and recruitment of Unc5B. Proceedings of the National Academy of
681 Sciences 105, 12491–12496. https://doi.org/10.1073/pnas.0804008105
682 Liebl, D.J., Klesse, L.J., Tessarollo, L., Wohlman, T., Parada, L.F., 2000. Loss of brain-derived neurotrophic
683 factor-dependent neural crest-derived sensory neurons in neurotrophin-4 mutant mice.
684 Proceedings of the National Academy of Sciences 97, 2297–2302.
685 https://doi.org/10.1073/pnas.040562597
686 Lindström, N.O., Guo, J., Kim, A.D., Tran, T., Guo, Q., De Sena Brandine, G., Ransick, A., Parvez, R.K.,
687 Thornton, M.E., Basking, L., Grubbs, B., McMahon, J.A., Smith, A.D., McMahon, A.P., 2018.
688 Conserved and Divergent Features of Mesenchymal Progenitor Cell Types within the Cortical
689 Nephrogenic Niche of the Human and Mouse Kidney. J Am Soc Nephrol 29, 806–824.
690 https://doi.org/10.1681/ASN.2017080890
691 Liu, J., Edgington-Giordano, F., Dugas, C., Abrams, A., Katakam, P., Satou, R., Saifudeen, Z., 2017.
692 Regulation of Nephron Progenitor Cell Self-Renewal by Intermediary Metabolism. J Am Soc
693 Nephrol 28, 3323–3335. https://doi.org/10.1681/ASN.2016111246
694 Liu, Y., Stein, E., Oliver, T., Li, Y., Brunken, W.J., Koch, M., Tessier-Lavigne, M., Hogan, B.L.M., 2004. Novel
695 Role for Netrins in Regulating Epithelial Behavior during Lung Branching Morphogenesis. Curr
696 Biol 14, 897–905. https://doi.org/10.1016/j.cub.2004.05.020
697 Lu, X., Le Noble, F., Yuan, L., Jiang, Q., De Lafarge, B., Sugiyama, D., Bréant, C., Claes, F., De Smet, F.,
698 Thomas, J.-L., Autiero, M., Carmeliet, P., Tessier-Lavigne, M., Eichmann, A., 2004. The netrin
699 receptor UNC5B mediates guidance events controlling morphogenesis of the vascular system.
700 Nature 432, 179–186. https://doi.org/10.1038/nature03080

701 Miyazaki, Y., Oshima, K., Fogo, A., Hogan, B.L., Ichikawa, I., 2000. Bone morphogenetic protein 4
702 regulates the budding site and elongation of the mouse ureter. J Clin Invest 105, 863–873.
703 https://doi.org/10.1172/JCI8256
704 Molema, G., Aird, W.C., 2012. Vascular Heterogeneity in the Kidney. Seminars in Nephrology,
705 Endothelium and the Kidney 32, 145–155. https://doi.org/10.1016/j.semnephrol.2012.02.001
706 Moore, M.W., Klein, R.D., Fariñas, I., Sauer, H., Armanini, M., Phillips, H., Reichardt, L.F., Ryan, A.M.,
707 Carver-Moore, K., Rosenthal, A., 1996. Renal and neuronal abnormalities in mice lacking GDNF.
708 Nature 382, 76–79. https://doi.org/10.1038/382076a0
709 Morizane, R., Lam, A.Q., Freedman, B.S., Kishi, S., Valerius, M.T., Bonventre, J.V., 2015. Nephron
710 organoids derived from human pluripotent stem cells model kidney development and injury.
711 Nat Biotechnol 33, 1193–1200. https://doi.org/10.1038/nbt.3392
712 Munro, D.A.D., Hohenstein, P., Davies, J.A., 2017. Cycles of vascular plexus formation within the
713 nephrogenic zone of the developing mouse kidney. Sci Rep 7, 3273.
714 https://doi.org/10.1038/s41598-017-03808-4
715 Nakagawa, N., Xin, C., Roach, A.M., Naiman, N., Shankland, S.J., Ligresti, G., Ren, S., Szak, S., Gomez, I.G.,
716 Duffield, J.S., 2015. Dicer1 activity in the stromal compartment regulates nephron
717 differentiation and vascular patterning during mammalian kidney organogenesis. Kidney Int 87,
718 1125–1140. https://doi.org/10.1038/ki.2014.406
719 O'Brien, L.L., Guo, Q., Bahrami-Samani, E., Park, J.-S., Hasso, S.M., Lee, Y.-J., Fang, A., Kim, A.D., Guo, J.,
720 Hong, T.M., Peterson, K.A., Lozanoff, S., Raviram, R., Ren, B., Fogelgren, B., Smith, A.D., Valouev,
721 A., McMahon, A.P., 2018. Transcriptional regulatory control of mammalian nephron progenitors
722 revealed by multi-factor cistromic analysis and genetic studies. PLoS Genet 14, e1007181.
723 https://doi.org/10.1371/journal.pgen.1007181
724 O'Brien, L.L., Guo, Q., Lee, Y., Tran, T., Benazet, J.-D., Whitney, P.H., Valouev, A., McMahon, A.P., 2016.
725 Differential regulation of mouse and human nephron progenitors by the Six family of
726 transcriptional regulators. Development 143, 595–608. https://doi.org/10.1242/dev.127175
727 Pallone, T.L., Zhang, Z., Rhinehart, K., 2003. Physiology of the renal medullary microcirculation. American
728 Journal of Physiology-Renal Physiology 284, F253–F266.
729 https://doi.org/10.1152/ajprenal.00304.2002
730 Pichel, J.G., Shen, L., Sheng, H.Z., Granholm, A.C., Drago, J., Grinberg, A., Lee, E.J., Huang, S.P., Saarma,
731 M., Hoffer, B.J., Sariola, H., Westphal, H., 1996. Defects in enteric innervation and kidney
732 development in mice lacking GDNF. Nature 382, 73–76. https://doi.org/10.1038/382073a0
733 Potente, M., Mäkinen, T., 2017. Vascular heterogeneity and specialization in development and disease.
734 Nat Rev Mol Cell Biol 18, 477–494. https://doi.org/10.1038/nrm.2017.36
735 Queisser, A., Seront, E., Boon, L.M., Vikkula, M., 2021. Genetic Basis and Therapies for Vascular
736 Anomalies. Circulation Research 129, 155–173.
737 https://doi.org/10.1161/CIRCRESAHA.121.318145
738 Reddi, V., Zaglul, A., Pentz, E.S., Gomez, R.A., 1998. Renin-expressing cells are associated with branching
739 of the developing kidney vasculature. J Am Soc Nephrol 9, 63–71.
740 https://doi.org/10.1681/ASN.V9163
741 Renier, N., Wu, Z., Simon, D.J., Yang, J., Ariel, P., Tessier-Lavigne, M., 2014. iDISCO: a simple, rapid
742 method to immunolabel large tissue samples for volume imaging. Cell 159, 896–910.
743 https://doi.org/10.1016/j.cell.2014.10.010
744 Ryan, A.R., England, A.R., Chaney, C.P., Cowdin, M.A., Hiltabidle, M., Daniel, E., Gupta, A.K., Oxburgh, L.,
745 Carroll, T.J., Cleaver, O., 2021. Vascular deficiencies in renal organoids and ex vivo kidney
746 organogenesis. Dev Biol 477, 98–116. https://doi.org/10.1016/j.ydbio.2021.04.009
747 Salminen, M., Meyer, B.I., Bober, E., Gruss, P., 2000. Netrin 1 is required for semicircular canal formation
748 in the mouse inner ear. Development 127, 13–22. https://doi.org/10.1242/dev.127.1.13

749 Sánchez, M.P., Silos-Santiago, I., Frisén, J., He, B., Lira, S.A., Barbacid, M., 1996. Renal agenesis and the
750 absence of enteric neurons in mice lacking GDNF. Nature 382, 70–73.
751 https://doi.org/10.1038/382070a0
752 Self, M., Lagutin, O.V., Bowling, B., Hendrix, J., Cai, Y., Dressler, G.R., Oliver, G., 2006. Six2 is required for
753 suppression of nephrogenesis and progenitor renewal in the developing kidney. EMBO J 25,
754 5214–5228. https://doi.org/10.1038/sj.emboj.7601381
755 Sequeira Lopez, M.L.S., Cherñavvsky, D.R., Nomasa, T., Wall, L., Yanagisawa, M., Gomez, R.A., 2003. The
756 embryo makes red blood cell progenitors in every tissue simultaneously with blood vessel
757 morphogenesis. American Journal of Physiology-Regulatory, Integrative and Comparative
758 Physiology 284, R1126–R1137. https://doi.org/10.1152/ajpregu.00543.2002
759 Sequeira-Lopez, M.L.S., Lin, E.E., Li, M., Hu, Y., Sigmund, C.D., Gomez, R.A., 2015a. The earliest
760 metanephric arteriolar progenitors and their role in kidney vascular development. Am J Physiol
761 Regul Integr Comp Physiol 308, R138–R149. https://doi.org/10.1152/ajpregu.00428.2014
762 Sequeira-Lopez, M.L.S., Nagalakshmi, V.K., Li, M., Sigmund, C.D., Gomez, R.A., 2015b. Vascular versus
763 tubular renin: role in kidney development. Am J Physiol Regul Integr Comp Physiol 309, R650–
764 R657. https://doi.org/10.1152/ajpregu.00313.2015
765 Serafini, T., Kennedy, T.E., Gaiko, M.J., Mirzayan, C., Jessell, T.M., Tessier-Lavigne, M., 1994. The netrins
766 define a family of axon outgrowth-promoting proteins homologous to C. elegans UNC-6. Cell 78,
767 409–424. https://doi.org/10.1016/0092-8674(94)90420-0
768 Smeyne, R.J., Klein, R., Schnapp, A., Long, L.K., Bryant, S., Lewin, A., Lira, S.A., Barbacid, M., 1994. Severe
769 sensory and sympathetic neuropathies in mice carrying a disrupted Trk/NGF receptor gene.
770 Nature 368, 246–249. https://doi.org/10.1038/368246a0
771 Srinivasan, K., Strickland, P., Valdes, A., Shin, G.C., Hinck, L., 2003. Netrin-1/neogenin interaction
772 stabilizes multipotent progenitor cap cells during mammary gland morphogenesis. Dev Cell 4,
773 371–382. https://doi.org/10.1016/s1534-5807(03)00054-6
774 Stanco, A., Szekeres, C., Patel, N., Rao, S., Campbell, K., Kreidberg, J.A., Polleux, F., Anton, E.S., 2009.
775 Netrin-1–α3β1 integrin interactions regulate the migration of interneurons through the cortical
776 marginal zone. Proceedings of the National Academy of Sciences 106, 7595–7600.
777 https://doi.org/10.1073/pnas.0811343106
778 Sun, K.L.W., Correia, J.P., Kennedy, T.E., 2011. Netrins: versatile extracellular cues with diverse functions.
779 Development 138, 2153–2169. https://doi.org/10.1242/dev.044529
780 Taguchi, A., Kaku, Y., Ohmori, T., Sharmin, S., Ogawa, M., Sasaki, H., Nishinakamura, R., 2014. Redefining
781 the In Vivo Origin of Metanephric Nephron Progenitors Enables Generation of Complex Kidney
782 Structures from Pluripotent Stem Cells. Cell Stem Cell 14, 53–67.
783 https://doi.org/10.1016/j.stem.2013.11.010
784 Takahashi, N., Lopez, M.L.S.S., Cowhig, J.E., Taylor, M.A., Hatada, T., Riggs, E., Lee, G., Gomez, R.A., Kim,
785 H.-S., Smithies, O., 2005. Ren1c homozygous null mice are hypotensive and polyuric, but
786 heterozygotes are indistinguishable from wild-type. J Am Soc Nephrol 16, 125–132.
787 https://doi.org/10.1681/ASN.2004060490
788 Takasato, M., Er, P.X., Chiu, H.S., Maier, B., Baillie, G.J., Ferguson, C., Parton, R.G., Wolvetang, E.J., Roost,
789 M.S., Chuva de Sousa Lopes, S.M., Little, M.H., 2015. Kidney organoids from human iPS cells
790 contain multiple lineages and model human nephrogenesis. Nature 526, 564–568.
791 https://doi.org/10.1038/nature15695
792 Tu, T., Zhang, C., Yan, H., Luo, Y., Kong, R., Wen, P., Ye, Z., Chen, J., Feng, J., Liu, F., Wu, J.Y., Yan, X.,
793 2015. CD146 acts as a novel receptor for netrin-1 in promoting angiogenesis and vascular
794 development. Cell Res 25, 275–287. https://doi.org/10.1038/cr.2015.15

795 Wälchli, T., Bisschop, J., Carmeliet, P., Zadeh, G., Monnier, P.P., De Bock, K., Radovanovic, I., 2023.
796 Shaping the brain vasculature in development and disease in the single-cell era. Nat Rev
797 Neurosci 1–28. https://doi.org/10.1038/s41583-023-00684-y
798 Wang, H., Copeland, N.G., Gilbert, D.J., Jenkins, N.A., Tessier-Lavigne, M., 1999. Netrin-3, a mouse
799 homolog of human NTN2L, is highly expressed in sensory ganglia and shows differential binding
800 to netrin receptors. J Neurosci 19, 4938–4947. https://doi.org/10.1523/JNEUROSCI.19-12-
801 04938.1999
802 Wilson, B.D., Ii, M., Park, K.W., Suli, A., Sorensen, L.K., Larrieu-Lahargue, F., Urness, L.D., Suh, W., Asai, J.,
803 Kock, G.A.H., Thorne, T., Silver, M., Thomas, K.R., Chien, C.-B., Losordo, D.W., Li, D.Y., 2006.
804 Netrins promote developmental and therapeutic angiogenesis. Science 313, 640–644.
805 https://doi.org/10.1126/science.1124704
806 Wu, H., Uchimura, K., Donnelly, E.L., Kirita, Y., Morris, S.A., Humphreys, B.D., 2018. Comparative Analysis
807 and Refinement of Human PSC-Derived Kidney Organoid Differentiation with Single-Cell
808 Transcriptomics. Cell Stem Cell 23, 869-881.e8. https://doi.org/10.1016/j.stem.2018.10.010
809 Yebra, M., Montgomery, A.M.P., Diaferia, G.R., Kaido, T., Silletti, S., Perez, B., Just, M.L., Hildbrand, S.,
810 Hurford, R., Florkiewicz, E., Tessier-Lavigne, M., Cirulli, V., 2003. Recognition of the Neural
811 Chemoattractant Netrin-1 by Integrins α6β4 and α3β1 Regulates Epithelial Cell Adhesion and
812 Migration. Developmental Cell 5, 695–707. https://doi.org/10.1016/S1534-5807(03)00330-7
813

814 **Figure Legends**

815 **Figure 1. *Ntn1* is expressed and secreted by stromal progenitors in the kidney and deletion**
816 **results in kidney hypoplasia**

817 (A) Light microscopy image of an E15.5 section showing the *in situ* hybridization expression
818 pattern of *Ntn1*. *Ntn1* expression is observed in the stromal progenitors (SP) surrounding the
819 nephron progenitors (NP). Dotted lines demarcate NP niches. Scale bar=50 µm. (B)
820 Immunostaining of E11.5 kidney sections shows that netrin-1 (magenta) is secreted by the
821 stromal progenitors surrounding the Six2+ (green) nephron progenitors. Inset shows a higher
822 magnification of the netrin-1 signal adjacent to the nephron progenitors. Scale bar=50 µm. (C)
823 Immunofluorescence images showing netrin-1 (magenta) signal in the stromal progenitors (SP)
824 and adjacent to the Six2+ nephron progenitors (NP, green) (left panel). Secreted netrin-1 signal
825 is also observed in the ureteric tip region. Genetic deletion of *Ntn1* in the *Foxd1*+ stromal

826 population results in a significant reduction in netrin-1 signal (right panel). Scale bar=25 μm. (D)
827 Kidney hypoplasia is observed at various stages of development. Shown are micrographs of
828 whole urogenital systems at E15.5 and P0. Insets for P0 show the same kidneys micro dissected
829 and side-by-side for size comparison. (E) Kidney length was measured in Fiji imaging software at
830 E13.5 and E15.5, with the size reduction becoming statistically significant by E15.5. Columns
831 and error represent mean and standard deviation (SD), respectively, with significance derived
832 from Students' T-test. Respective p-values displayed on graphs.

833 **Figure 2. Loss of *Ntn1* delays the cessation of nephrogenesis but is not due to signaling**
834 **through nephron progenitor expressed *Unc5c* or differences in progenitor dynamics**

835 A) Immunostaining of whole metanephric kidneys at E11.5 shows that metanephric kidney
836 development is initiated normally in *Ntn1* conditional knockouts, with the expected T-shaped
837 ureteric bud (cytokeratin, magenta) surrounded by condensed nephron progenitors (Six2,
838 green). Scale bar=200 μm. B) Nephron progenitor niches (Six2, green) appear normally
839 organized at E15.5 in surface views of wholemount immunostained kidneys. Scale bar=30 μm.
840 C) Wholemount immunostains of P4 kidneys show the persistence of Six2+ nephron progenitors
841 (green) on the surface of the kidney in *Ntn1* conditional knockouts. Scale bar=30 μm. D) *In situ*
842 hybridization showing the expression of the netrin-1 receptor *Unc5c* in the nephron progenitors
843 (black arrowhead), podocytes (yellow arrowhead), and smooth muscle layer of the ureter
844 (green arrowhead) at E15.5. Scale bar=50 μm. E) Light microscopy images of whole kidneys at
845 P0 showing no difference in kidney size of *Unc5c* knockout kidneys compared to controls. F)
846 Wholemount immunostaining and surface views show the normal organization of nephron

847 progenitor niches in *Unc5c* knockouts at P0 (Six2-green, cytokeratin-magenta). Scale bar=40
848 µm. G) Example of a sectioned kidney labeled with EdU (white) and immunostained with Six2
849 (green) and E-cadherin (Ecad, magenta) to label the nephron progenitors and collecting duct
850 system, respectively. Inset shows a high magnification image of a niche with dotted lines
851 highlighting the extent of what was considered either a nephron progenitor (NP) niche or
852 ureteric bud (UB) tip niche for quantification purposes. Scale bar=200 µm. H) Quantification of
853 Six2+ nephron progenitors or Ecad+ ureteric tip cells at E13.5, E15.5, and P0 show no significant
854 differences in total cell numbers except for Ecad+ cells at E13.5. Bars represent mean;
855 significance was determined using Students t-test. I) Quantification of the % of EdU+ Six2+
856 nephron progenitors or EdU+ Ecad+ ureteric tip cells reveals no significant difference at E13.5,
857 E15.5, or P0 between *Foxd1*$^{GC/+}$; *Ntn1*$^{fl/fl}$ kidneys or controls. Bars represent mean; significance
858 was determined using Students t-test.

859 **Figure 3. Stromal deletion of *Ntn1* results in aberrant neurovascular patterning**

860 A) *In situ* hybridization on E15.5 kidney sections shows the expression of the netrin-1 receptor
861 *Unc5b* in the endothelium of the kidney (black arrowhead and inset of glomerular endothelium,
862 left panel), the secondary branches/generations of the collecting duct (yellow arrowhead, left
863 panel), and ureter (right panel). Scale bars=50 µm B) Wholemount immunostain of an E15.5
864 wildtype kidney show the tracking of Tuj1+ (cyan) axonal projections with the renal vasculature
865 (CD31, red). Far right panel shows an independent close-up image of a neurovascular bundle.
866 Merge scale bar=300 µm, close-up scale bar=50 µm. C) Wholemount immunostains show the
867 organization of the nerves and vasculature at E15.5 in *Nnt1* conditional knockouts and controls.

868 The nerves (Tuj1, cyan) track with the endothelium (CD31, red) in all genotypes. White
869 arrowheads highlight the abnormal patterning observed in *Ntn1* conditional mutants such as
870 looping and ectopic neurovascular bundles. Scale bar=300 μm. D) Depiction of tracing (white
871 lines) of the neurovascular bundles (left panel). Tracing of five control kidneys (top panel,
872 colored lines) show predictable patterns of 5 main lateral arterial branches which can be
873 overlayed. *Ntn1* conditional knockout kidneys (bottom panel, colored lines) show stochastic
874 patterning with the absence of any predictable patterning. Scale bar=300 μm. E) Wholemount
875 immunostains of control, $TrkA^{-/-}$, and $Foxd1^{GC/+}$; $Ntn1^{fl/fl}$; $TrkA^{-/-}$ kidneys at E16.5 show the
876 organization of nerves (Tuj1, cyan), endothelium (CD31, red), and smooth muscle cells (SMA,
877 green). Innervation of the kidney is reduced in *TrkA* knockouts, but abnormal patterning
878 persists with vasculature not associated with axons (arrowheads) still showing abnormal
879 patterning, suggesting the endothelium is the primary responder to netrin-1 guidance cues.
880 Scale bar=300 μm.

881 **Figure 4. *Ntn1* conditional knockouts have normal endothelial metrics but reduced smooth**
882 **muscle coverage throughout development**

883 A) Quantitation of CD31+ endothelial metrics including the number of branches, branch points,
884 and total endothelium (total additive length, μM) at E15.5 shows no statistical differences
885 between controls and *Ntn1* conditional knockouts. Significance was calculated with Students t-
886 test, $p<0.05$ was considered significant, columns represent mean. Error bars = SD. B)
887 Wholemount immunostaining of E15.5 kidneys with smooth muscle actin (SMA, green) in
888 addition to the axonal (Tuj1, cyan) and endothelial (CD31, red) markers show a qualitative delay

889 in smooth muscle cell association with the endothelium (white arrowheads, zoom) suggesting a
890 potential delay is vascular maturation. Scale bars=300 μm. C) Wholemount immunostains of
891 E15.5 and P0 kidneys with SMA (white) show a qualitative reduction on SMA vascular coverage
892 in *Ntn1* conditional mutants. The injection of Evans Blue dye at 2 months to label the adult
893 kidney vasculature shows a well-developed arterial tree with some remnants of abnormal
894 patterning such as elongated branches in *Ntn1* conditional knockouts. Red dotted lines overlay
895 normal (top) and abnormal (bottom) branching. E15.5 scale bar=300 μm, P0 scale bar=500 μm,
896 2-month scale bar=1000 μm. D) Quantitation of SMA+ arterial metrics including the number of
897 branches, branch points, and total vasculature length (μM) at E15.5 and P0 show a deficit in
898 smooth muscle metrics suggesting a delay in arterial differentiation. Quantitation of Evans blue
899 labeled arterial vascular metrics at 2 months reveals that *Ntn1* conditional knockouts have
900 attained levels similar to controls. Significance was calculated with Students t-test, $p<0.05$ was
901 considered significant, individual p-values are displayed on the respective graphs, while
902 columns represent mean. Error bars = SD. Demarcation between P0 and two months denotes
903 the differences in labeling, with early stages labeled by SMA and 2 months perfused with Evans
904 blue.

905 **Figure 5. Gene expression analyses support a delay in vascular maturation in *Ntn1* conditional**
906 **knockouts**

907 A) Gene ontology (GO) analysis of genes upregulated (top) or B) downregulated (bottom) in
908 *Ntn1* conditional knockouts. Shown are the GO Biological Processes enriched in both categories.
909 Genes were considered up- or downregulated with a >1.2 fold-change. In the insets are

910 examples of genes that are upregulated (top) or downregulated (bottom). C) Schematic of the

911 role of netrin-1 in guiding vascular patterning and maturation during development.

Figure 1

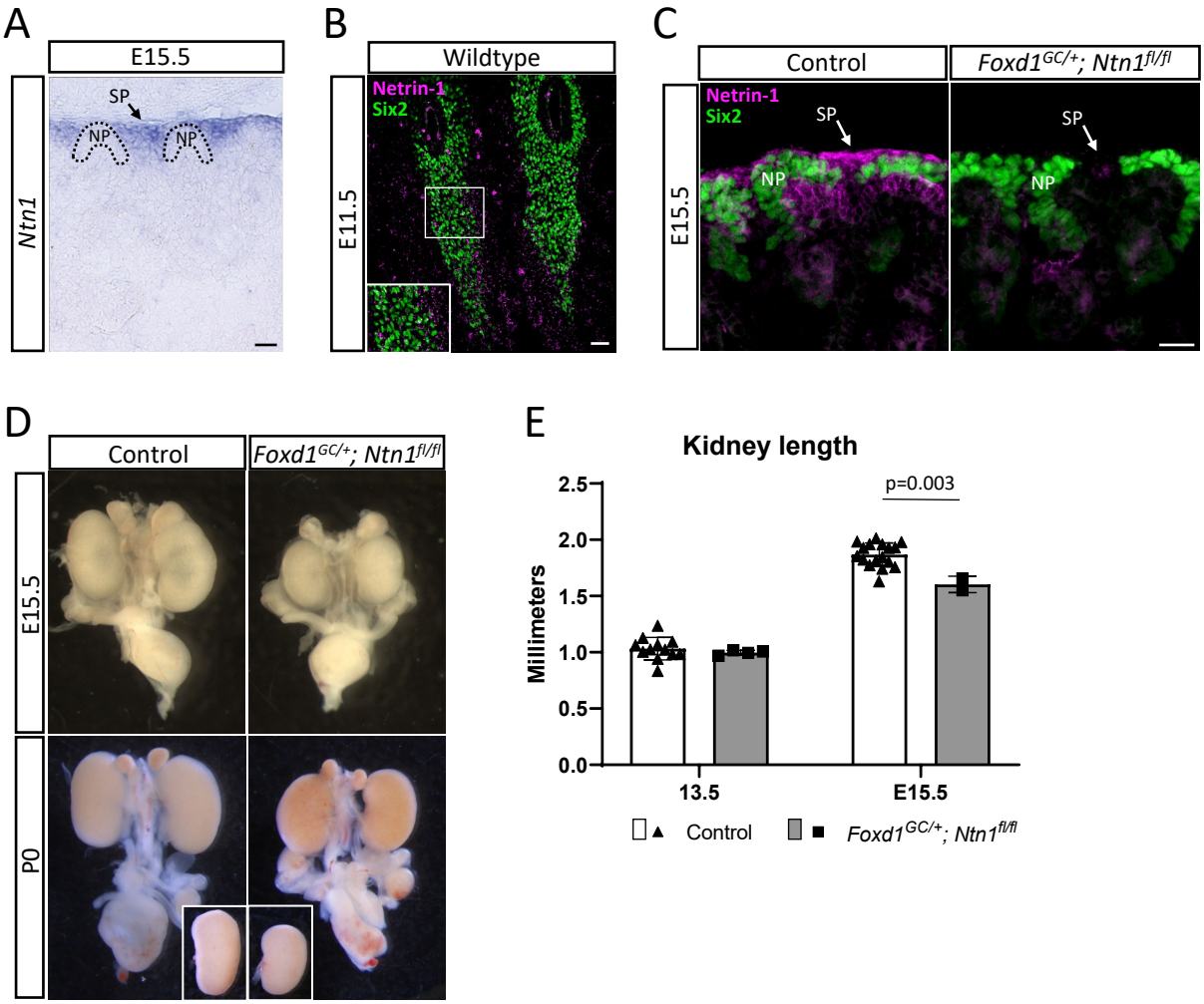
A
E15.5
Ntn1
SP
NP
NP
B
Wildtype
E11.5
Netrin-1
Six2
C
Control
Foxd1GC/+; Ntn1fl/fl
E15.5
Netrin-1
Six2
SP
NP
SP
NP
D
Control
Foxd1GC/+; Ntn1fl/fl
E15.5
P0
E
Kidney length
p=0.003
Millimeters
2.5
2.0
1.5
1.0
0.5
0.0
13.5
E15.5
Control
Foxd1GC/+; Ntn1fl/fl

Figure 2

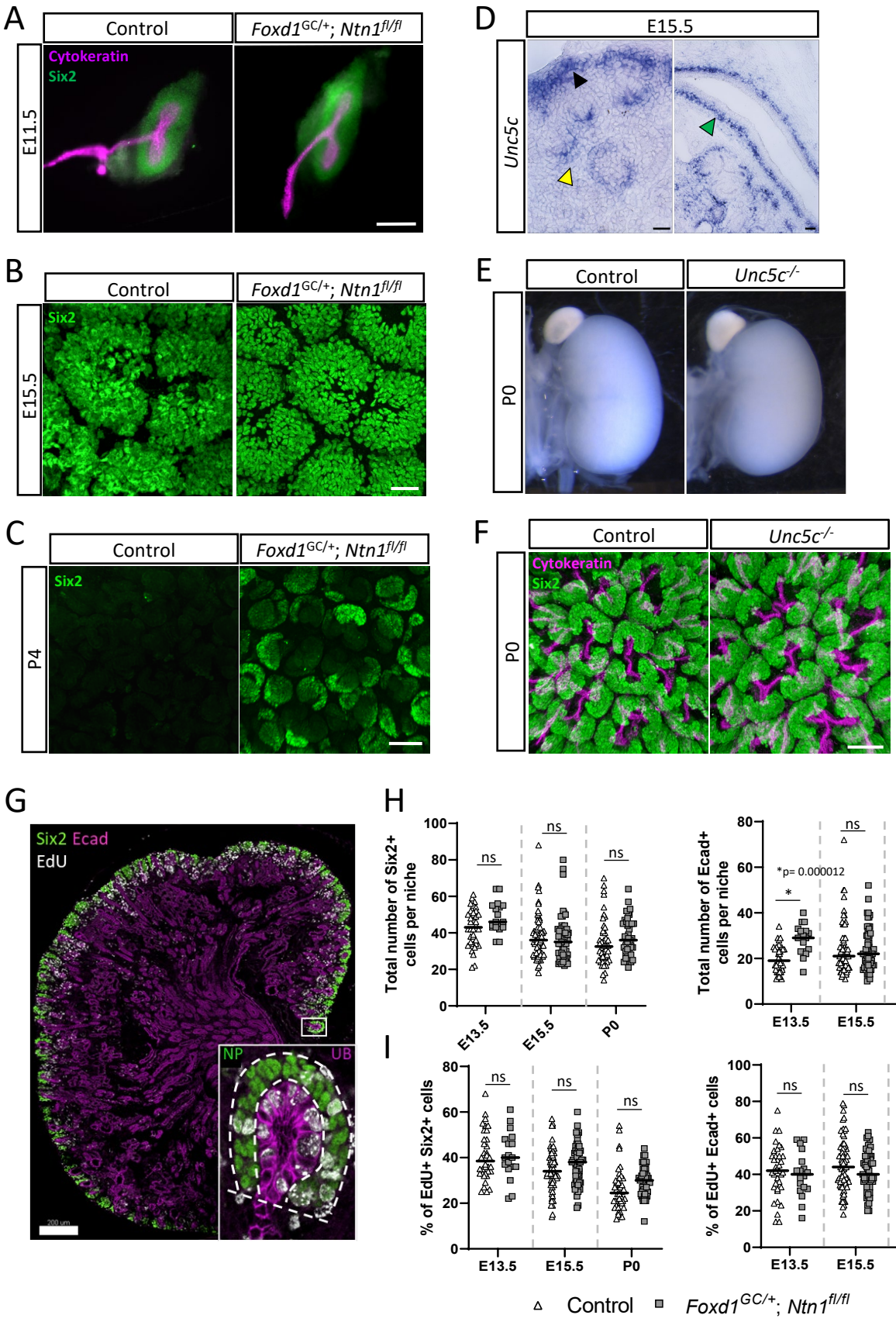
A
Control
Foxd1GC/+; Ntn1fl/fl
E11.5
Cytokeratin
Six2
B
Control
Foxd1GC/+; Ntn1fl/fl
E15.5
Six2
C
Control
Foxd1GC/+; Ntn1fl/fl
P4
Six2
D
E15.5
Unc5c
E
Control
Unc5c-/-
P0
F
Control
Unc5c-/-
P0
Cytokeratin
Six2
G
Six2 Ecad
EdU
NP
UB
200 um
H
Total number of Six2+ cells per niche
Total number of Ecad+ cells per niche
ns
*p= 0.000012
*
E13.5
E15.5
P0
I
% of EdU+ Six2+ cells
% of EdU+ Ecad+ cells
Control
Foxd1GC/+; Ntn1fl/fl

Figure 3

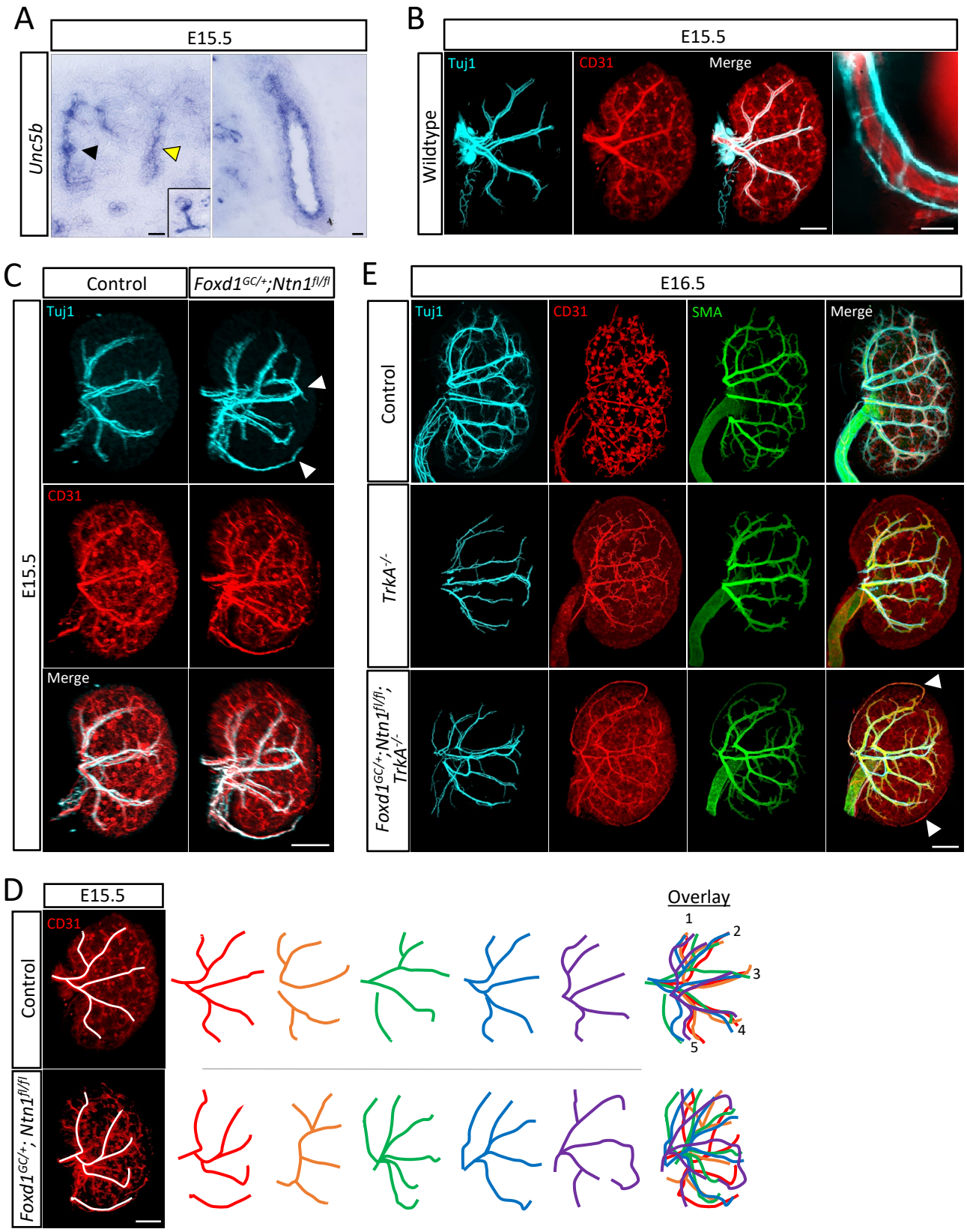
A
E15.5
Unc5b
B
E15.5
Wildtype
Tuj1
CD31
Merge
C
Control
Foxd1GC/+;Ntn1fl/fl
E15.5
Tuj1
CD31
Merge
E
E16.5
Control
TrkA-/-
Foxd1GC/+;Ntn1fl/fl; TrkA-/-
Tuj1
CD31
SMA
Merge
D
E15.5
Control
Foxd1GC/+; Ntn1fl/fl
CD31
Overlay
1
2
3
4
5

Figure 4

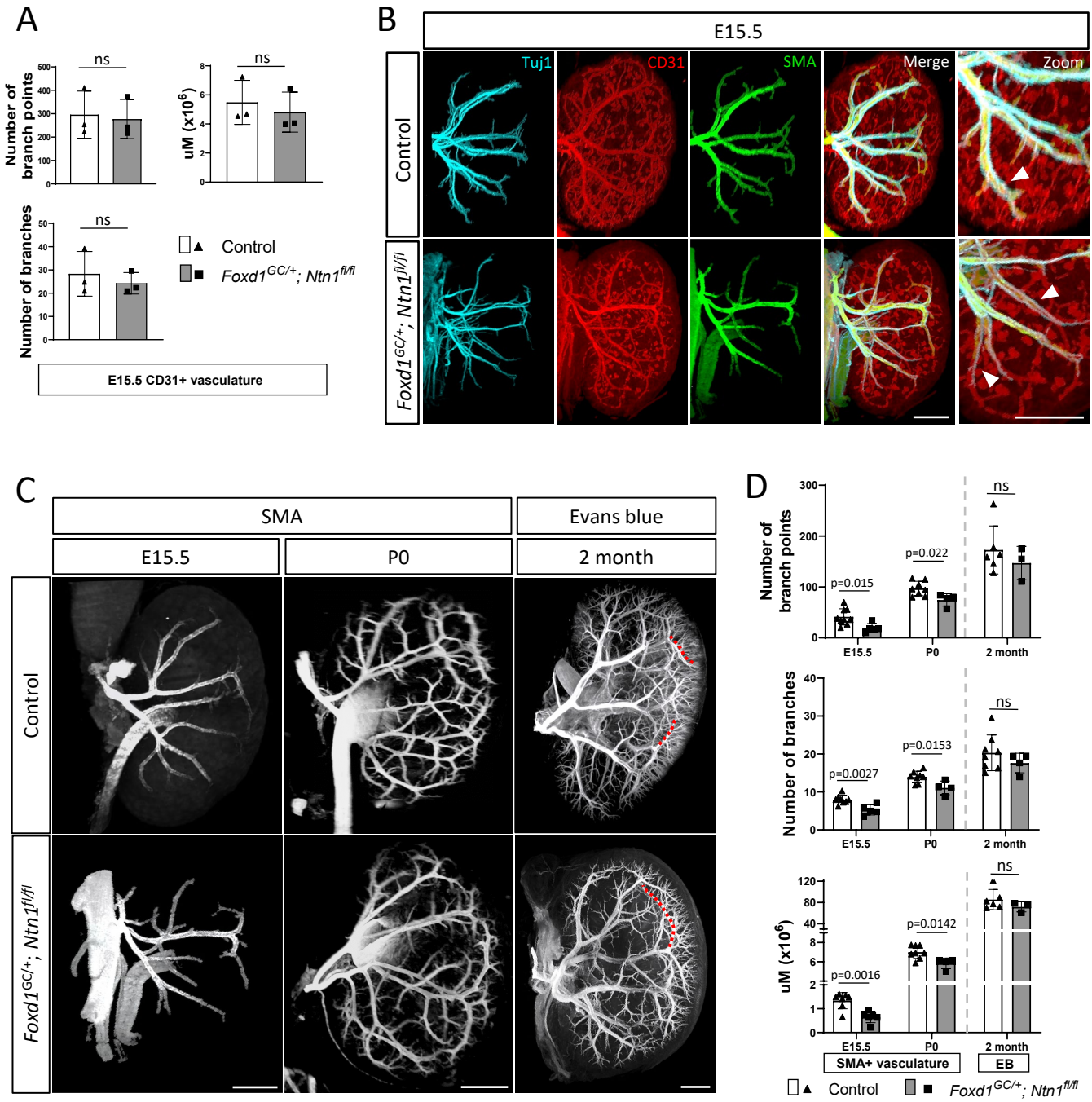
A
ns
Number of branch points
uM (x10^6)
Number of branches
Control
Foxd1^GC/+; Ntn1^fl/fl
E15.5 CD31+ vasculature
B
E15.5
Tuj1
CD31
SMA
Merge
Zoom
Control
Foxd1^GC/+; Ntn1^fl/fl
C
SMA
Evans blue
E15.5
P0
2 month
Control
Foxd1^GC/+; Ntn1^fl/fl
D
Number of branch points
p=0.015
p=0.022
ns
E15.5
P0
2 month
Number of branches
p=0.0027
p=0.0153
uM (x10^6)
p=0.0016
p=0.0142
SMA+ vasculature
EB
Control
Foxd1^GC/+; Ntn1^fl/fl

Figure 5

A

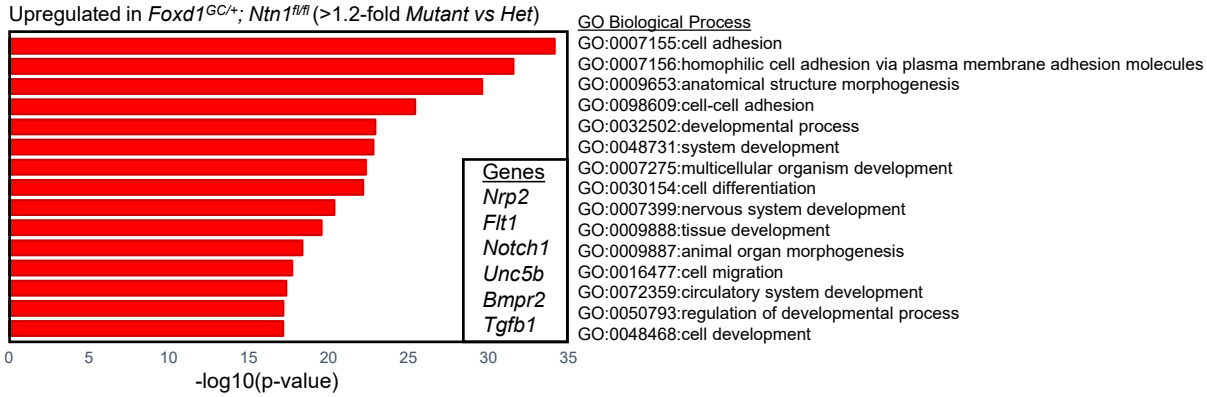
Upregulated in Foxd1GC/+; Ntn1fl/fl (>1.2-fold Mutant vs Het)
GO Biological Process
GO:0007155:cell adhesion
GO:0007156:homophilic cell adhesion via plasma membrane adhesion molecules
GO:0009653:anatomical structure morphogenesis
GO:0098609:cell-cell adhesion
GO:0032502:developmental process
GO:0048731:system development
GO:0007275:multicellular organism development
GO:0030154:cell differentiation
GO:0007399:nervous system development
GO:0009888:tissue development
GO:0009887:animal organ morphogenesis
GO:0016477:cell migration
GO:0072359:circulatory system development
GO:0050793:regulation of developmental process
GO:0048468:cell development
Genes
Nrp2
Flt1
Notch1
Unc5b
Bmpr2
Tgfb1
0
5
10
15
20
25
30
35
-log10(p-value)

B

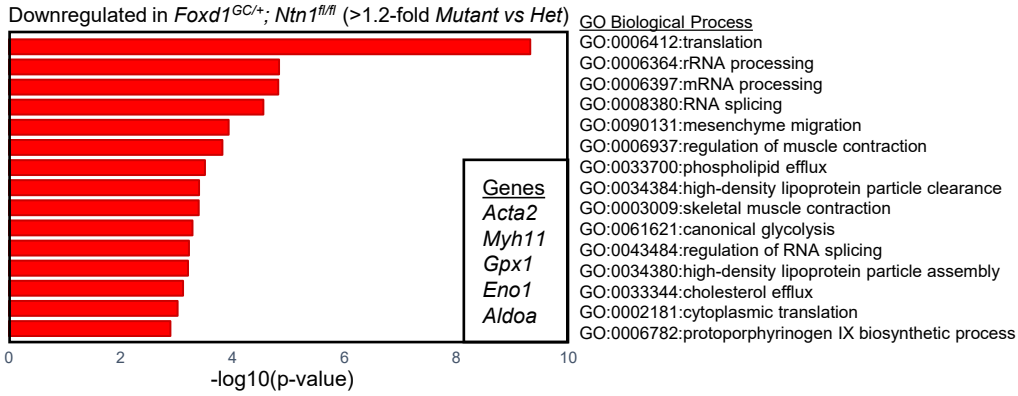
Downregulated in Foxd1GC/+; Ntn1fl/fl (>1.2-fold Mutant vs Het)
GO Biological Process
GO:0006412:translation
GO:0006364:rRNA processing
GO:0006397:mRNA processing
GO:0008380:RNA splicing
GO:0090131:mesenchyme migration
GO:0006937:regulation of muscle contraction
GO:0033700:phospholipid efflux
GO:0034384:high-density lipoprotein particle clearance
GO:0003009:skeletal muscle contraction
GO:0061621:canonical glycolysis
GO:0043484:regulation of RNA splicing
GO:0034380:high-density lipoprotein particle assembly
GO:0033344:cholesterol efflux
GO:0002181:cytoplasmic translation
GO:0006782:protoporphyrinogen IX biosynthetic process
Genes
Acta2
Myh11
Gpx1
Eno1
Aldoa
0
2
4
6
8
10
-log10(p-value)

C

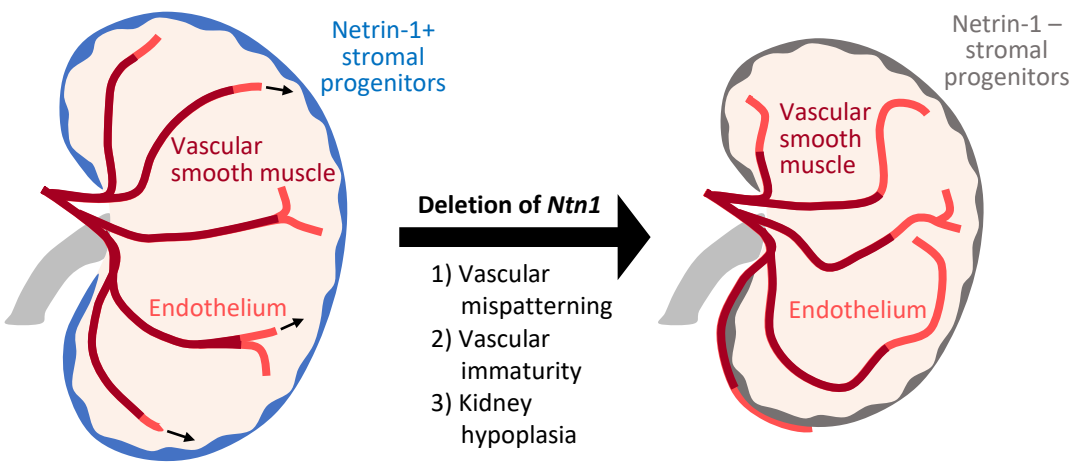
Netrin-1+
stromal
progenitors
Vascular
smooth muscle
Endothelium
Deletion of Ntn1
1) Vascular
mispatterning
2) Vascular
immaturity
3) Kidney
hypoplasia
Netrin-1 –
stromal
progenitors
Vascular
smooth
muscle
Endothelium